JAERI-M
87-029

TRANSPORT ANALYSIS OF OH AND NBI HEATED DISCHARGES IN JT-60

March 1987

Toshio HIRAYAMA, Katsuhiro SHIMIZU, Mitsuru KIKUCHI
Hiroshi SHIRAI and JT-60 Team

日本原子力研究所
Japan Atomic Energy Research Institute

JAERI-Mレポートは，日本原子力研究所が不定期に公刊している研究報告書です。
入手の問合わせは，日本原子力研究所技術情報部情報資料課（〒319-11茨城県那珂郡東海村）あて，お申しこしください。なお，このほかに財団法人原子力弘済会資料センター（〒319-11 茨城県那珂郡東海村日本原子力研究所内）で複写による実費頒布をおこなっております。

JAERI-M reports are issued irregularly.
Inquiries about availability of the reports should be addressed to Information Division Department of Technical Information, Japan Atomic Energy Research Institute, Tokai-mura, Naka-gun, Ibaraki-ken 319-11, Japan.

©Japan Atomic Energy Research Institute, 1987

編集兼発行　日本原子力研究所
印　　刷　㈱高野高速印刷

JAERI-M 87-029

Transport Analysis of OH and NBI Heated Discharges in JT-60

Toshio HIRAYAMA, Katsuhiro SHIMIZU, Mitsuru KIKUCHI,
Hiroshi SHIRAI and JT-60 Team

Department of Large Tokamak Research
Naka Fusion Research Establishment
Japan Atomic Energy Research Institute
Naka-machi, Naka-gun, Ibaraki-ken

(Received January 30, 1987)

Transport properties of ohmically and NBI heated plasmas in JT-60 have been analysed by using the one-dimensional tokamak transport code. The very flat density profiles observed in ohmic heating discharges are explained by no inward flow velocity of hydrogen. The saturation of the energy confinement time at high density discharges is due to the increase of the ion energy loss channel and the combination of the neoclassical ion heat diffusivity χ_i^{CH} with multiplication factor of around 6 and the electron heat diffusivity $\chi_e = 5 \times 10^{19}/n_e q$ well reproduces experimental data in the density range of $\bar{n}_e = (2 \sim 8) \times 10^{19}$ m^{-3}. The analysis also shows that the electrical conductivity has the Spitzer-type dependence and the trapped electron correction is small. The degradation of the energy confinement under the high power NBI heating is due to the enhancement of electron heat diffusivity. For discharges with 20 MW NBI heating, electron heat diffusivity increases to $\chi_e = 5$ m^2/s at $\bar{n}_e = 5 \times 10^{19}$ m^{-3}. By taking into account the beam pressure, it was also shown that stored energies evaluated by the magnetic analysis is consistent with the value evaluated from the transport analysis.

Keywords: Tokamak, JT-60, Ohmic Heating, NBI Heating, Energy Confinement Time, Resistivity, LOOK, SCOOP, LIBRARY

JT-60 Team

* T.ABE, H.AIKAWA, N.AKAOKA, H.AKASAKA, M.AKIBA, N.AKINO, T.AKIYAMA, T.ANDO, K.ANNOH, N.AOYAGI, T.ARAI, K.ARAKAWA, M.ARAKI, K.ARIMOTO, M.AZUMI, S.CHIBA, M.DAIRAKU, N.EBISWA, T.FUJII, T. FUKUDA, H.FURUKAWA, K.HAMAMATSU, K.HAYASHI, M.HARA, K.HARAGUCHI, H.HIRATSUKA, T.HIRAYAMA, S.HIROKI, K.HIRUTA, M.HONDA, H.HORIIKE, R.HOSODA, N.HOSOGANE, Y.IIDA, T.IIJIMA, K.IKEDA, Y.IKEDA, T.IMAI, T.INOUE,, N.ISAJI, M.ISAKA, S.ISHIDA, N.ITIGE, T.ITO, Y.ITO, A.KAMINAGA, M.KAWAI, Y.KAWAMATA, K.KAWASAKI, K.KIKUCHI, M.KIKUCHI, H.KIMURA, T.KIMURA, H.KISHIMOTO, K.KITAHARA, S.KITAMURA, A.KITSUNEZAKI, K.KIYONO, N.KOBAYASHI, K.KODAMA, Y.KOIDE, T.KOIKE, M.KOMATA, I.KONDO, S.KONOSHIMA, H.KUBO, S.KUNIEDA, S.KURAKATA, K.KURIHARA, M.KURIYAMA, T.KURODA, M.KUSAKA, Y.KUSAMA,, S.MAEHARA, K.MAENO, S.MATSUDA, S.MASE, M.MATSUKAWA, T.MATSUKAWA, M.MATSUOKA, N.MIYA, K.MIYATI, Y.MIYO, K.MIZUHASHI, M.MIZUNO, R.MURAI, Y.MURAKAMI, M.MUTO, M.NAGAMI, A.NAGASHIMA, K.NAGASHIMA, T.NAGASHIMA, S.NAGAYA, H.NAKAMURA, Y.NAKAMURA, M.NEMOTO, Y.NEYATANI, S.NIIKURA, H.NINOMIYA, T.NISHITANI, H.NOMATA, K.OBARA, N.OGIWARA, T.OHGA, Y.OHARA, K.OHASA, H.OHHARA, T.OHSHIMA, M.OHKUBO, K.OHTA, M.OHTA, M.OHTAKA, Y.OHUCHI, A.OIKAWA, H.OKUMURA, Y.OKUMURA, K.OMORI, S.OMORI, Y.OMORI, T.OZEKI, A.SAKASAI, S.SAKATA, M.SATOU, M.SAIGUSA, K.SAKAMOTO, M.SAWAHATA, M.SEIMIYA, M.SEKI, S.SEKI, K.SHIBANUMA, R.SHIMADA, K.SHIMIZU, M.SHIMIZU, Y.SHIMOMURA, S.SHINOZAKI, H.SHIRAI, H.SHIRAKATA, M.SHITOMI, K.SUGANUMA, T.SUGIE, T.SUGIYAMA, H.SUNAOSHI, K.SUZUKI, M.SUZUKI, M.SUZUKI, N.SUZUKI, S.SUZUKI, Y.SUZUKI, M.TAKAHASHI, S.TAKAHASHI, T.TAKAHASHI, H.TAKAHASHI**, M.TAKASAKI, M.TAKATSU, H.TAKEUCHI, A.TAKESHITA, S.TAMURA, S.TANAKA, T.TANAKA, K.TANI, M.TERAKADO, T.TERAKADO, K.TOBITA, T.TOKUTAKE, T.TOTSUKA, N.TOYOSHIMA, H.TSUDA, T.TSUGITA, S.TSUJI, Y.TSUKAHARA, M.TSUNEOKA, K.UEHARA, M.UMEHARA, Y.URAMOTO, H.USAMI, K.USHIGUSA, K.USUI, J.YAGYU, K.YAMADA, M.YAMAMOTO, O.YAMASHITA, Y.YAMASHITA, K.YANO, T.YASUKAWA, K.YOKOKURA, H.YOKOMIZO, K.YOSHIKAWA, M.YOSHIKAWA, H.YOSHIDA, Y.YOSHINARI, R.YOSHINO, I.YONEKAWA, K.WATANABE

ＯＨ及びＮＢＩ加熱時のＪＴ－６０プラズマの輸送解析

日本原子力研究所那珂研究所臨界プラズマ研究部
平山俊雄・清水勝宏・菊池　満・白井　浩
ＪＴ－６０チーム

（１９８７年１月３０日受理）

一次元トカマク輸送コート・シミュレーションによって，ＪＴ－６０におけるＯＨ及びＮＢＩ加熱プラズマの輸送特性を解析した。

ＯＨプラズマにおけるエネルギー閉じ込め時間のプラズマ密度上昇に併う飽和現象は，イオン系からのエネルギー損失が支配的となるためであり，イオン熱伝導率が新古典理論の６倍程度あると仮定すると，計算結果は実験結果を良く表現できる。又，プラズマの電気伝導率は古典的であり，捕捉電子効果は小さいことが示された。

ＮＢＩ加熱に併うエネルギー閉じ込め時間の劣化は，電子熱伝導率の増加によるものであり，２０ＭＷ入射の場合，χ_e の値は５m^2/s（$\bar{n}_e = 5\times10^{19} m^{-3}$）迄増大している事がわかった。又，ビーム粒子のエネルギー密度を考慮すると，平衡から評価された蓄積エネルギーとプラズマ密度及び温度から評価した蓄積エネルギーは良い一致をみることが示された。

那珂研究所：〒311－02 茨城県那珂郡那珂町大字向山801－1

相川 裕史、青柳 哲雄、赤岡 伸雄、赤坂 博美、秋野 昇、秋場 真人、秋山 隆、安積 正史、
阿部 哲也、新井 貴、荒川喜代次、荒木 政則、有本 公子、安東 俊郎、安納 勝人、飯島 勉、
飯田 幸生、池田 幸治、池田 佳隆、井坂 正義、伊佐治信明、石田 真一、市毛 尚志、伊藤 孝雄、
伊藤 康浩、井上多加志、今井 剛、上原 和也、宇佐美広次、牛草 健吉、薄井 勝富、梅原 昌敏、
浦本 保幸、海老沢 昇、及川 晃、大麻 和美、大内 豊、大賀 徳道、大久保 実、大島 貴幸、
太田 和也、太田 充、大高 光夫、大原比呂志、大森憲一郎、大森 俊造、大森 栄和、荻原 徳男、
奥村 裕司、奥村 義和、小関 隆久、小原建治郎、小原 祥裕、神永 敦嗣、河合視己人、川崎 幸三、
川俣 陽一、菊池 勝美、菊池 満、岸本 浩、北原 勝美、北村 繁、狐崎 晶雄、木村 豊秋、
木村 晴行、清野 公廣、日下 誠、草間 義紀、国枝 俊介、久保 博孝、倉形 悟、栗原 研一、
栗山 正明、黒田 猛、小池 常之、小出 芳彦、児玉 幸三、木島 滋、小林 則幸、小又 将夫、
近藤 育朗、三枝 幹雄、逆井 章、坂田 信也、坂本 慶司、佐藤 正泰、沢畠 正之、部 守正、
篠崎 信一、柴沼 清、嶋田 隆一、清水 勝宏、清水 正亜、下村 安夫、白井 浩、白形 弘文、
菅沼 和明、杉江 達夫、杉山 隆、鈴木 貞明、鈴木 國弘、鈴木 紀男、鈴木 正信、鈴木 道雄、
鈴木 康夫、砂押 秀則、清宮 宗孝、関 省吾、関 正美、高崎 学、高津 英幸、高橋 春次、
高橋虎之助、高橋 弘法、高橋 実、竹内 浩、竹下 明、田中 茂、田中竹次郎、谷 啓二、
田村 早苗、大楽 正幸、千葉 真一、塚原 美光、次田 友宣、辻 俊二、津田 文男、恒岡まさき、
寺門 恒久、寺門 正之、徳竹 利国、戸塚 俊之、飛田 健次、豊島 昇、中村 博雄、中村 幸治、
長島 章、永島 圭介、永島 孝、永谷 進、永見 正幸、新倉 節夫、西谷 健夫、二宮 博正、
根本 正博、関谷 譲、野亦 英幸、浜松 清隆、林 和夫、原 誠、原口 和三、平塚 一、
平山 俊雄、蛭田 和治、広木 成治、福田 武司、藤井 常幸、古川 弘、細金 延幸、細田隆一郎、
堀池 寛、本田 正男、前野 勝樹、前原 直、間瀬 修次、松岡 守、松川 達哉、松川 誠、
松田慎三郎、水野 誠、水橋 清、宮 直之、宮地 謙吾、三代 康彦、武藤 貢、村井 隆一、
村上 義夫、柳生 純一、安川 亨、矢野 勝久、山下 修、山下 幸彦、山田喜美雄、山本 正弘、
横倉 賢治、横溝 英明、吉川 和伸、吉川 允二、吉田 英俊、吉成 洋治、芳野 隆治、米川 出、
渡辺 和弘、

Contents

目　　次

1. Introduction

The study of plasma confinement in a large tokamak is the key issue of the fusion reactor development. In JT-60, ohmically and neutral beam heated plasmas have been extensively studied in the wide range of plasma density and heating power [1,2,3]. The line averaged electron density has been stably increased up to $\bar{n}_e=8\times10^{19}m^{-3}$ in ohmic discharges and the neutral beam power was increased up to 20 MW with plasma current of $I_p=1.0\sim2.0$ MA. Clean plasmas with effective charge number of $Z_{eff}=1\sim2$ and flat density profiles were obtained both for divertor and limiter discharges. The confinement analysis shows that the gross energy confinement time of the ohmically heated plasma saturates at density $\bar{n}_e\sim4\times10^{19}m^{-3}$ and is weakly dependent on the plasma density and the plasma current above this threshold density. The neutral beam heating degrades the energy confinement with heating power as L-mode discharges but the dependence of the confinement time on the plasma density and the plasma current is still very weak as the one in ohmic discharges [4].

In this paper, we study the above-mentioned confinement properties of ohmically and neutral beam heated plasmas in JT-60 from the viewpoint of transport code analysis. In the next section, we analyse the transport process in ohmic discharges. The density profile and the effective charge number of the plasma are also studied in this section. In the section 3, discharges under high power NBI heating are analysed. And results of transport simulation in JT-60 are summarized in the section 4.

2. Ohmically Heated Discharges

2.1 Experimental data

The experimental data are taken by selecting a plasma current I_p and the scanning a range of the line averaged electron density $\bar{n}_e$ up to $\sim8\times10^{19}$ m^{-3} for ohmically heated plasmas in JT-60. Hydrogen and helium plasmas are chosen for the various density scans in the divertor or limiter discharges. In this session, we will present the profile characteristics of the electron temperature and density and the energy

1. Introduction

The study of plasma confinement in a large tokamak is the key issue of the fusion reactor development. In JT-60, ohmically and neutral beam heated plasmas have been extensively studied in the wide range of plasma density and heating power [1,2,3]. The line averaged electron density has been stably increased up to $\bar{n}_e=8\times10^{19}m^{-3}$ in ohmic discharges and the neutral beam power was increased up to 20 MW with plasma current of $I_p=1.0\sim2.0$ MA. Clean plasmas with effective charge number of $Z_{eff}=1\sim2$ and flat density profiles were obtained both for divertor and limiter discharges. The confinement analysis shows that the gross energy confinement time of the ohmically heated plasma saturates at density $\bar{n}_e\sim4\times10^{19}m^{-3}$ and is weakly dependent on the plasma density and the plasma current above this threshold density. The neutral beam heating degrades the energy confinement with heating power as L-mode discharges but the dependence of the confinement time on the plasma density and the plasma current is still very weak as the one in ohmic discharges [4].

In this paper, we study the above-mentioned confinement properties of ohmically and neutral beam heated plasmas in JT-60 from the viewpoint of transport code analysis. In the next section, we analyse the transport process in ohmic discharges. The density profile and the effective charge number of the plasma are also studied in this section. In the section 3, discharges under high power NBI heating are analysed. And results of transport simulation in JT-60 are summarized in the section 4.

2. Ohmically Heated Discharges

2.1 Experimental data

The experimental data are taken by selecting a plasma current I_p and the scanning a range of the line averaged electron density $\bar{n}_e$ up to $\sim8\times10^{19}$ m^{-3} for ohmically heated plasmas in JT-60. Hydrogen and helium plasmas are chosen for the various density scans in the divertor or limiter discharges. In this session, we will present the profile characteristics of the electron temperature and density and the energy

confinement properties for ohmically heated plasmas.

Figure 1 shows the variation of central electron temperature and resistive voltage V_p with the line averaged electron density. The central electron temperature rapidly decreases as the density increases to around $2\sim3\times10^{19}$ m^{-3} and is gradually on the decay above that density. The resistive voltage becomes to be high $\sim0.6V$ *to* $\sim1V$ with the density but does not show the non-linear increase. The resistive voltage which is important to estimate the ohmic input power accurately is defined by

$$V_l = V_p + \frac{1}{2}I_p\dot{L}_i \tag{1}$$

where V_l is the loop voltage and L_i the internal inductance. Although the discharge duration of JT-60 is about 10 sec, the effect of temporal evolution of L_i can not be neglected at a high plasma current(2 MA), leading to an uncertainty in the V_p of less than 10 %, except for discharges with a large $\dot{n}_e$. From Shafranov $\Lambda(=\beta_p+l_i/2)$ measured by the equilibrium, the time derivative of L_i is expressed as

$$\dot{L}_i = \mu_0 R(\dot{\Lambda} - \dot{\beta}_p) \tag{2}$$

where μ_0 is the vacuum permeability, R the major radius and β_p the beta poloidal. The time evolution of β_p is approximated by

$$\dot{\beta}_p = \int_0^a (\dot{p}_e(r) + \dot{p}_i(r))dV/(VB_p^2/2\mu_0) \tag{3}$$

$$\dot{p}_e(r) = \dot{n}_e(0)f_{ne}(r)T_e(r) + n_e(r)\dot{T}_e(0)f_{Te}(r),$$

$$\dot{p}_i(r) = \dot{n}_i(0)f_{ni}(r)T_i(r) + n_i(r)\dot{T}_i(0)f_{Ti}(r),$$

where $\dot{n}_e(0)$ and $\dot{T}_e(0)$ are measured by FIR and ECE diagnostics, respectively, and $f_n(r)$ and $f_T(r)$ are normalized profiles for density and temperature. The time derivative of ion pressure is approximated from electron parameters, assuming $\dot{T}_i(0)=\dot{T}_e(0)$ and $\dot{n}_i(0)=\dot{n}_e(0)$.

The change of the electron temperature profile and the electron

density profile are shown in Fig.2 as a function of the electron density. The axis of ordinates presents the ratio of the central to the volume averaged. The electron temperature profile does not change up to a high density of $\sim 8\times 10^{19} m^{-3}$, though indicating the amount of scatter large in the low density. At the low density, the electron density profile for the limiter discharge is more peaked than the one for the divertor discharges. With the increment of the density, both profiles become broad and show no remarkable difference in their shapes.

We can now calculate the energy confinement time defined as

$$\tau_E = \frac{W_e + W_i}{V_p I_p - (\dot{W}_e + \dot{W}_i)}, \tag{4}$$

where W_e and W_i are, respectively, kinetic energies of the electrons and ions integrated over the plasma volume. The experimental profiles of T_e and n_e are input to the time independent code LOOK/SCOOP [5] together with the global parameters I_p, V_l, B_t, etc. In the steady transport analysis, ion temperature profile is calculated by employing the neoclassical ion heat diffusivity proposed by Chang-Hinton [6] with the enhancement factor of 3. The power transport from the electrons to the ions is calculated by the classical formula. The power loss due to convection is obtained from the inferred particle flux and the charge exchange loss from the neutral penetration calculation with assumed particle confinement time of 100 ms. Ion density depletion is estimated by using the resistive Z_{eff} (see §2.2) and by assuming carbon is the only impurity. Figure 3 shows the dependence of τ_E on electron density and $\tau_E^* = \bar{n}_e R^2 a q_{cy}$ scaled with Neo-Alcator, where a is the minor radius and q_{cy} the cylindrical safety factor. It is seen from these figures that τ_E saturates at about 0.4 sec above around $n_e \sim 4\times 10^{19} m^{-3}$ or $\tau_E^* = 1\times 10^{21}$. There are little differences in the energy confinement times between hydrogen and helium plasmas and also between limiter and divertor discharges. Although τ_E observed in JET [7] linearly increases with τ_E^*, the data of TFTR [8] begin to saturate at τ_E^* of 0.5×10^{21} and present the τ_E of $\sim 0.4 sec$, which is almost the same value as the one in JT-60.

2.2 Plasma Resistivity during quasi-steady State

The plasma resistivity $\eta_{//}$ in the quasi-steady state is important in determining the electron energy balance. As have been mentioned uncertainties in the plasma resistivity [9,10,11,12], two kinds of formula are used i.e. Spitzer resistivity and the neoclassical one with trapping correction [13]. In the calculation of the resistivity, Z_{eff} is obtained by iteration to obtain agreement with the ohmic input power, followed by

$$I_p V_p = \int_0^a \eta_{//}(Z_{eff}, T_e(r)) J_z(r)^2 dV, \tag{5}$$

in which $J_z(r)$ is the toroidal current density. In the following, we have used the two types of current density profile. The first one is estimated from the usual assumption of the constant electric field over the radius,

$$J_z(r) = \frac{E_z}{\eta_{//}(Z_{eff}, T_e(r))}. \tag{6}$$

Another model of $J_z(r)$ is represented by

$$J_z(r) = J_0(1-(\frac{r}{a})^2)^{\alpha}. \tag{7}$$

The central current density J_0 is given by assuming $q(0)=1$ and the value of α is obtained by making the internal inductance meat to the measured one. As using the eq.(6), large amount of scatter of $T_e(r)$ at the low density (Fig.2) lead to an uncertainty in the resistive Z_{eff}. Therefore, the eq.(7) is employed through this work. Both resistive Z_{eff} from two different J_z agree well, as reducing the scatter of $T_e(r)$ at the high density.

The dependence of resistive Z_{eff} on the electron density is shown in Fig.4. As using the Spitzer formula, the resistive Z_{eff} rapidly decreases with the increase of electron density from $1\times10^{19}m^{-3}$ to $2\sim3\times10^{19}m^{-3}$ and shows the reasonable values less than 1.5 ($\bar{n}_e \geqq 4\times10^{19}m^{-3}$). On the other hand, the neoclassical resistivity

results in $Z_{eff}<1$ in hydrogen discharges and $Z_{eff}<2$ in helium discharges, as shown in Fig. 4-b. Especially at the high density, some discharges frequently failed to estimate the resistive Z_{eff}, because the value of Z_{eff} is so small that the trapping correction becomes to be negative. In order to make Z_{eff} value of 0.5 above unity, the electron temperature must increase by 60%. This fact is apparently out of the error for the electron temperature. Figure 5 shows the value of Z_{eff} measured by visible bremsstrahlung [3] as a function of the electron density at I_P=1.0~1.5 MA for the divertor discharges and the limiter discharges. The measured Z_{eff} shows the good agreement with the resistive Z_{eff} from Spitzer formula. These results strongly suggest that the trapped particle correction to the resistivity should be reduced or suppressed.

2.3 Simulation of Ohmically Heated Plasmas

The computer simulation are carried out with the LIBRARY transport code [14] and concentrate more on the flat density profile and the saturated energy confinement time.

In many other tokamaks, the experimentally observed profiles of electron densities have a nearly parabolic or Gaussian shape in the inner region of the plasma column. An anomalous inward flux of the form $-2n_eDr/a^2$ [15] is introduced and successfully explains such density profiles. In JT-60, flat density profiles showing $n_e(0)/<n_e>$=1.1~1.2 are realized for middle- and high density discharges, though peaked profiles like a parabolic shape are seen in limiter discharges at the low density. The characteristics of the density profiles are satisfactorily simulated with no anomalous inward flux and differences in cold neutral energy. In Figs 6 and 7, computed density profiles are compared with the measurements. The anomalous inward flux (shown in broken-line) leads to more peaked density profiles for both limiter and divertor discharges. The differences in cold neutral energies i.e. E_0=5eV for divertor discharges and E_0=30eV for limiter discharges, could be responsible for the observed differences in n_e profiles at low densities. This is because that cold neutrals which directly recycle with limiter have a higher energy of

dozens to hundred eV.

There are some candidates for the saturated energy confinement time. 1) Impurity radiation: Since the impurity radiation power for the divertor discharges is only 20~30 % of the input power, the radiation losses due to impurities should not be responsible for the τ_E saturation. 2) Convection loss : In a transient stage , the large diffusion coefficie of ~1 m^2/s was observed. This large diffusion coefficient is not employed in our simulation study, because there are no inward flux which must compensate for the large outward flux due to the large diffusion. 3) Electron heat diffusivity χ_e : Figure 8 shows the electron heat diffusivity χ_e^E estimated at a/3 for the observed profiles of the electron temperature and density for the plasma current of 2.0 MA, in which ion conduction loss is fixed to be 3 times the neoclassical ion heat diffusivity of Chang-Hinton and convection loss $3/2\Gamma T$. The INTOR scaling χ_e of $5\times10^{19}/n_e$ and the χ_e^{HP} measured by the heat pulse of the sawtooth are also shown in this figure. The χ_e^E is almost the same as χ_e^{HP}. It is reported that the χ_e^{HP} is greater than the χ_e^E by a factor of 10, because of including the convection loss [16]. Therefore, the χ_e can not be enhanced so as to cause the τ_e saturation. 4) Ion heat diffusivity χ_i : Figure 9 presents the experimental profile of the electron density and temperature for the shot of E1791 with I_P=1.5 MA. As the factor of 6 for χ_i^{CH} is taken, the χ_i is the same as the χ_e^E over the radius. This result shows that the ion energy loss catches up with the electron energy loss at the high density regime and also suggests that the enhanced ion heat diffusivity may be responsible for the τ_E saturation.

Figure 10 shows the simulation results for E1791 (I_P=1.5MA) based on the following empirical transport coefficients,

$\chi_e=5\times10^{19}/n_e q_{cy}$,

$\chi_i=6\chi_i^{CH}$,

$D=1\times10^{19}/n_e$,

Spitzer resistivity,

Spitzer resistivity,
no anomalous inward flux,
cold neutral energy of 5 eV.

The plasma profiles at the low density of $2.5\times10^{19}m^{-3}$ are presented in Fig. 10-a ; the temperature profiles of electron and ion, the profiles of electron density and safety factor q. Figure 10-b shows the profiles at the high density of $6.6\times10^{19}m^{-3}$. The calculated electron temperature profiles are in good agreement with the observed temperature denoted in open circles, although the central temperature is slightly decreased due to the sawtooth effect.

Figure 11 shows the simulation results for 2MA discharge (E1709) based on the same transport mentioned above. Figures 11-a and -b correspond to the cases at the density of $6.0\times10^{19}m^{-3}$ and of $7.5\times10^{19}m^{-3}$, respectively. The used transport parameters yield good fits with the observed T_e profiles within error bars.

We show the τ_E versus the electron density, comparing with the calculated τ_E shown in solid lines in Fig. 12. As for the plasma parameters with I_P=2.0MA, in Fig. 12-a, the calculated τ_E is good agreements in the experimental values at the low density ($\bar{n}_e\leqq3\times10^{19}m^{-3}$) and shows a tendency toward the saturation. As for the plasma with I_P=1.5MA, in Fig. 12-b, the calculated τ_E also shows good agreement with the experiments on both the τ_E value and the tendency of the τ_E saturation. The assumption that ion loss channel becomes dominant in energy loss channels at the high density brings about good agreement with the experimental measurements.

3. Simulation of NBI Heated Plasmas

The degradation of the electron diffusivity χ_e during NB heating phase is estimated by using the tokamak transport code. The power deposition profile of the Neutral Beam Injection and the stored fast ion energy are calculated in detail by using the Orbit Following Monte Carlo code (OFMC code) [5]. We also estimated the charge exchange loss of fast ion for various neutral density profiles.

We analyzed a series of helium discharge with the beam power Pb=10 MW and a series of hydrogen discharge with Pb=20 MW. Time evolution of the parameters for relatively high density discharge $\bar{n}_e=5.4\times10^{19}m^{-3}$ and low density discharge $\bar{n}_e=2.4\times10^{19}m^{-3}$ are shown in Fig. 13 and Fig. 14, respectively. In both discharges, we observed the rapid saturation of the central electron temperature and the plasma stored energy estimated from the magnetic equilibrium measurement.

The local transport analysis assumed steady state (SCOOP result) shows that the electron heat diffusivity χ_e during NBI heating is about 3~5 m^2/s [4]. These estimated values are very sensitive to the local gradient of electron temperature dTe/dr. It is difficult to determine dTe/dr from the 6-point Thomson scattering measurement with 10~20 % error bars. So we estimated the electron heat diffusivity during NBI heating by using the prediction transport code.

The procedure of the simulation is as follows:

(1) The density profile is determined from 3-ch FIR data. Instead of solving the particle balance equation, this density profile is used in the simulation.

(2) The energy transfer from fast ions to bulk electron and ions are calculated by OFMC code. In this calculation the experimental data is used for plasma parameter, such as ne and Te. The neutral density profile is calculated by 2-Dimensional Neutral transport code [17]. The absolute value is determined assuming that the particle confinement time is 50 msec.

(3) We solve the time-dependent equations of electron and ion energy balance employing the INTOR scaling for the anomalous diffusion;

$$D=10^{19}/n_e$$

$$\chi_e = 5\times 10^{19}/n_e$$
$$\chi_i = 3\times \chi_i^{CH} \ .$$

(4) The electron heat diffusivity during NBI heating χ_e^{NB} is enhanced by a factor 2-4.

$$\chi_e^{NB} = f_e \times \chi_e^{INTOR}$$

At first, we carried out the simulation for helium discharge with Pb=10 MW. The content ratio of hydrogen ion in helium plasma is not clear. But the amount of the beam shine through in helium discharge is less than that in hydrogen discharge with same densities. This fact indicates that the helium ion content is larger than hydrogen ion. So the density ratio of helium and hydrogen n_{He}/n_H is assumed to be 2.0 in the calculation of beam deposition. We used the cross section for He^{++} ionization which scales as Z^2 times the proton ionization, where Z is the charge number of ion [18].

Figure 15(a) shows the density dependence of the stored energy of fast ions. The incremental stored energy estimated from the magnetic measurement ΔW_{mag}, which include the contribution from the fast ions, and the incremental kinetic energy calculated from the plasma parameters ΔW_{kin} are also plotted in this figure. The ratio of beam components to the incremental stored energy decreases with the electron density. For low density discharges with $\bar{n}_e < 3\times 10^{19}\ m^{-3}$, the beam component is dominant in the incremental stored energy. The agreement between the thermal energy estimated from the magnetic measurement and from the kinetic method is fairy good. The density dependence of the partition of beam power is shown in Fig 15(b). For low density discharge with $\bar{n}_e < 2\times 10^{19}\ m^{-3}$, the major part of the beam power is lost by the shine-through and the charge exchange loss. The power deposited from the fast ions to the electrons is larger than that to the bulk ions because of the low electron temperature.

The charge exchange loss reduces the power deposited to ions. We estimated the C.X. loss for the various neutral density profile. The results are summarized in Table 1. When the particle confinement time τ_P is reduced from 50 msec to 30 msec, the C.X. loss increases from 12 % to 16 %. The change of neutral density profile due to the neutral energy is insignificant for the C.X. loss. In JT-60 divertor discharges, recycling neutrals are localized at the divertor side. This asymmetric neutral profile has no influence on C.X. loss. Figure

16 shows the density profile of halo neutral and recycling neutral. Halo neutrals contribute only to the neutral density at center and the recycling neutral dominate outer region. Most of the fast particle neutralized at center region are reionized. Therefore, the C.X. loss due to halo neutrals is negligible.

Figure 17 shows the power deposition profile calculated by OFMC code for E2151 and E2154 discharge. The deposition profile is hollow even for the low density discharge due to the off-axis injection and the very flat density profile.

Figure 18 shows the simulation result for E2154 discharge ($\bar{n}_e=5.4\times10^{19}\ m^{-3}, P_B=10MW$). We used the enhanced electron heat diffusivity $\chi_e^{NB}=2.\times\chi_e^{INTOR}$ during NBI heating. The electron temperature measured by Thomson Scattering at t=6.4 sec shows by the closed symbol. The simulation result is in good agreement with the experimental data. The broad temperature profile is due partly to the hollow deposition profile and partly to the homogeneous thermal diffusion χ_e in the core region.

Figure 19 shows the simulation result for E2151 discharge ($\bar{n}_e=2.4\times10^{19}m^{-3}, P_B=10MW$). This result indicated that the enhancement factor for low density must be smaller than 2 in order to reproduce the experimental data. As for the ion temperature, there is a possibility of the degradation of the ion energy confinement during NBI heating. However, it should be noted that the ion temperature measured by the doppler broadening of TiXXI is not always coincident with the central bulk ion temperature. Impurity transport analysis point out that the doppler broadening evaluate the central ion temperature too lower according to the impurity density profile [19]. So we did not make an effort to investigate the degradation of ion thermal diffusivity.

We also executed the simulation for the hydrogen discharge with high beam power Pb=20 MW. The incremental stored energy ΔW_{mag} and the stored fast ion energy W_b for several density scan are plotted in Fig. 20(a). Figure 20(b) shows the density dependence of the partition of beam power. In order to keep the shine through below 10 %, the line density must be higher than about $5\times10^{19}m^{-3}$. Figure 21 shows the experimental result and the simulation result by using χ_e^{NB} enhanced by a factor 4. INTOR scaling can not reproduce the density dependence of

the central electron temperature. In the high density region of $\bar{n}_e > 6\times10^{19} m^{-3}$, the difference between the simulation and the experiment is significant. This fact implies that the electron heat diffusivity during NBI phase has weak density dependence. In the middle density region of $\bar{n}_e = 5\times10^{19} m^{-3}$, where χ_e about 5 m^2/s, the simulation agrees with the experimental data fairly well. Comparing with the simulation of helium discharge with 10 MW, χ_e^{NB} seems to degrade with the beam power. We can conclude that the degradation of the confinement during NBI heating is due to enhanced electron heat diffusivity.

4. Summary

Transport properties of ohmically and NBI heated plasmas in JT-60 have been analysed by using the one-dimensional tokamak transport code. The very flat density profiles observed in ohmic heating discharges are explained by no inward flow velocity of hydrogen. The saturation of the energy confinement time at high density discharges is due to the increase of the ion energy loss channel and the combination of the neoclassical ion heat diffusivity χ_i^{CH} with multiplication factor of around 6 and the electron heat diffusivity $\chi_e = 5.\times10^{19}/n_e q$ well reproduces experimental data in the density range of $\bar{n}_e = (2 \sim 8)\times10^{19} m^{-3}$. The analysis also shows that the electrical conductivity has the Spitzer-type dependence and the trapped electron correction is small. The degradation of the energy confinement under the high power NBI heating is due to the enhancement of electron heat diffusivity. For discharges with 20 MW NBI heating, electron thermal conductivity increases to $\chi_e = 5\ m^2/s$ at $\bar{n}_e = 5.\times10^{19} m^{-3}$. By taking into account the beam pressure, it was also shown that stored energies evaluated by the magnetic analysis is consistent with the value evaluated from the transport analysis.

Acknowledgements

The authors wish to thank Drs. Y. Shimomura and M. Azumi for fruitful discussions. The continuing support of Drs. S. Mori, K. Tomabechi, M. Yoshikawa and T. Iijima, is gratefully acknowledged.

the central electron temperature. In the high density region of $\bar{n}_e > 6\times10^{19} m^{-3}$, the difference between the simulation and the experiment is significant. This fact implies that the electron heat diffusivity during NBI phase has weak density dependence. In the middle density region of $\bar{n}_e = 5\times10^{19} m^{-3}$, where χ_e about 5 m^2/s, the simulation agrees with the experimental data fairly well. Comparing with the simulation of helium discharge with 10 MW, χ_e^{NB} seems to degrade with the beam power. We can conclude that the degradation of the confinement during NBI heating is due to enhanced electron heat diffusivity.

4. Summary

Transport properties of ohmically and NBI heated plasmas in JT-60 have been analysed by using the one-dimensional tokamak transport code. The very flat density profiles observed in ohmic heating discharges are explained by no inward flow velocity of hydrogen. The saturation of the energy confinement time at high density discharges is due to the increase of the ion energy loss channel and the combination of the neoclassical ion heat diffusivity χ_i^{CH} with multiplication factor of around 6 and the electron heat diffusivity $\chi_e = 5.\times10^{19}/n_e q$ well reproduces experimental data in the density range of $\bar{n}_e = (2 \sim 8)\times10^{19} m^{-3}$. The analysis also shows that the electrical conductivity has the Spitzer-type dependence and the trapped electron correction is small. The degradation of the energy confinement under the high power NBI heating is due to the enhancement of electron heat diffusivity. For discharges with 20 MW NBI heating, electron thermal conductivity increases to $\chi_e = 5\ m^2/s$ at $\bar{n}_e = 5.\times10^{19} m^{-3}$. By taking into account the beam pressure, it was also shown that stored energies evaluated by the magnetic analysis is consistent with the value evaluated from the transport analysis.

Acknowledgements

The authors wish to thank Drs. Y. Shimomura and M. Azumi for fruitful discussions. The continuing support of Drs. S. Mori, K. Tomabechi, M. Yoshikawa and T. Iijima, is gratefully acknowledged.

the central electron temperature. In the high density region of $\bar{n}_e > 6\times10^{19} m^{-3}$, the difference between the simulation and the experiment is significant. This fact implies that the electron heat diffusivity during NBI phase has weak density dependence. In the middle density region of $\bar{n}_e = 5\times10^{19} m^{-3}$, where χ_e about 5 m^2/s, the simulation agrees with the experimental data fairly well. Comparing with the simulation of helium discharge with 10 MW, χ_e^{NB} seems to degrade with the beam power. We can conclude that the degradation of the confinement during NBI heating is due to enhanced electron heat diffusivity.

4. Summary

Transport properties of ohmically and NBI heated plasmas in JT-60 have been analysed by using the one-dimensional tokamak transport code. The very flat density profiles observed in ohmic heating discharges are explained by no inward flow velocity of hydrogen. The saturation of the energy confinement time at high density discharges is due to the increase of the ion energy loss channel and the combination of the neoclassical ion heat diffusivity χ_i^{CH} with multiplication factor of around 6 and the electron heat diffusivity $\chi_e = 5.\times10^{19}/n_e q$ well reproduces experimental data in the density range of $\bar{n}_e = (2 \sim 8)\times10^{19} m^{-3}$. The analysis also shows that the electrical conductivity has the Spitzer-type dependence and the trapped electron correction is small. The degradation of the energy confinement under the high power NBI heating is due to the enhancement of electron heat diffusivity. For discharges with 20 MW NBI heating, electron thermal conductivity increases to $\chi_e = 5\ m^2/s$ at $\bar{n}_e = 5.\times10^{19} m^{-3}$. By taking into account the beam pressure, it was also shown that stored energies evaluated by the magnetic analysis is consistent with the value evaluated from the transport analysis.

Acknowledgements

The authors wish to thank Drs. Y. Shimomura and M. Azumi for fruitful discussions. The continuing support of Drs. S. Mori, K. Tomabechi, M. Yoshikawa and T. Iijima, is gratefully acknowledged.

References

1) YOSHIKAWA, M. and JT-60 team, Plasma Physics and Controlled Nuclear Fusion Research, IAEA, Vienna, 1986, IAEA-CN-47/A-I-1

2) JT-60 team presented by M. NAGAMI, Plasma Physics and Controlled Nuclear Fusion Research, IAEA, Vienna, 1986, IAEA-CN-47/A-II-2

3) JT-60 team presented by H. TAKEUCHI, Plasma Physics and Controlled Nuclear Fusion Research, IAEA, Vienna, 1986, IAEA-CN-47/A-IV-3

4) KIKUCHI, M., HIRAYAMA, T., SHIMIZU, K. et al., "Incremental Energy Confinement Time during the H Beam Heating in JT-60", to be published in JAERI-M ,1987.

5) HIRAYAMA, T., SHIMIZU, K., TANI, K., KIKUCHI, M., et al., 'Experimental Transport Analysis System in JT-60', to be published in JAERI-M.

6) CHANG, C.S., HINTON, F.L., Phys. Fluids, 25 (1982) 1493.

7) JET Joint Undertaking Annual Report 1985, EUR 10615 EN, (1986).

8) EFTHIMION, P.C., BRETZ, N., BELL, M., et al., in Plasma Physics and Controlled Nuclear Fusion Research (Proc. 10th Int. Conf. London, 1984), Vol.1, IAEA, Vienna (1985) 29.

9) BOL, K., et al., in Plasma Physics and Controlled Nuclear Fusion Research (Proc. 7th Int. Conf. Insbruck, 1978), Vol.1, IAEA, Vienna (1979) 11.

10) EJIMA, S., PETRIE, T.W., RIVIERE, A.C., et al., Nucl. Fusion, 22 (1982) 1627.

11) MESERVEY, E., BITTER, M., DAUGHNEY, C., Nucl. Fusion, 24 (1984) 3.

12) BEHRINGER, K.H., ABELS-VON MAANEN, A., BONNERUS, J., et al., in Plasma Physics and Controlled Nuclear Fusion Research (Proc. 10th

Int. Conf. London, 1984), Vol.1, IAEA, Vienna (1985) 291.

13) HIRAYAMA, T., The Second US/Japan Work shop on Transport Simulation in Large Tokamaks (Princeton, 1985) ; HIRAYAMA, t., et al., Library system for a one dimensional tokamak transport code (in Japanese), Japan Atomic Energy Research Institute, Japan, Report No. JAERI-M 82-204 (1982).

14) HIRSHMAN, S.P., HAWRYLUK, R.J., BIRGE, B., Neoclassical conductivity of a Tokamak Plasma, PPPL-1326, (1977).

15) COPPI, B., SHARKY, N., Physics of Plasmas close to Thermonuclear Conditions (Proc. of the Course to Thermonuclear Conditions, Varenna, 1979),EUR-FU-BRUX/XII/476/80, (1980) 47.

16) FERDRICKSON, E.D., CALLEN, J.D., McGUIRE, K., et al., Nucl. Fusion 26 (1986) 849.

17) SHIMIZU, K. and AZUMI, M., "Two Dimensional Neutral Transport Analysis in Tokamak plasma", to be published in JAERI M (1987)

18) RIVIERE, A.C., Nucl. Fusion 11 (1971) 363.

19) KOIDE,Y., private communication.

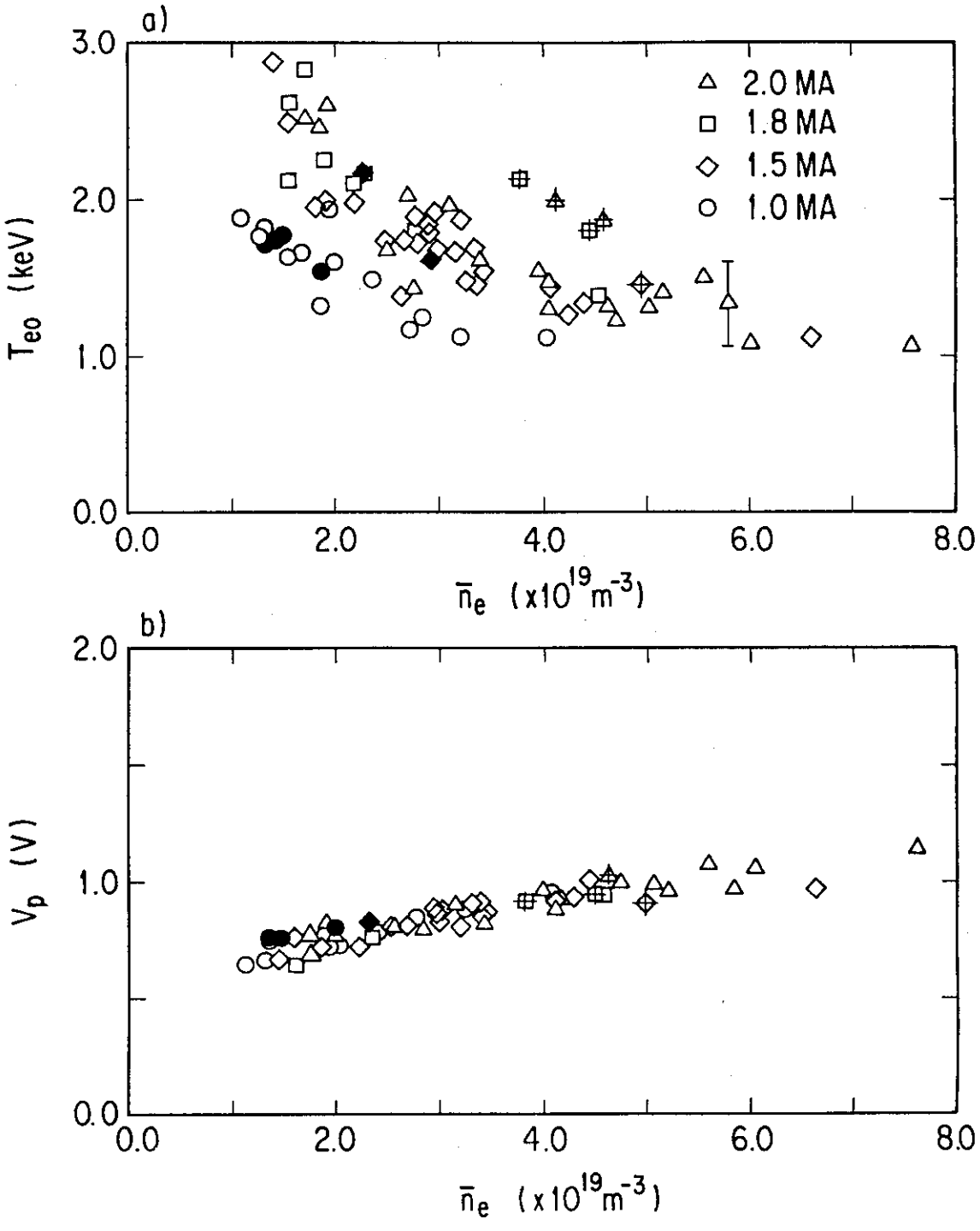

Fig. 1. a) The central electron temperatures versus the line averaged electron density. b) The resistive voltages versus the line averaged electron density. Circle means I_p=1.0MA, diamond I_p=1.5MA, tetragon I_p=1.8MA and triangle I_p=2.0MA. Open symbol and closed one present, respectively, the hydrogen divertor discharges and the hydrogen limiter discharges. Symbol with '+' means the helium divertor discharges.

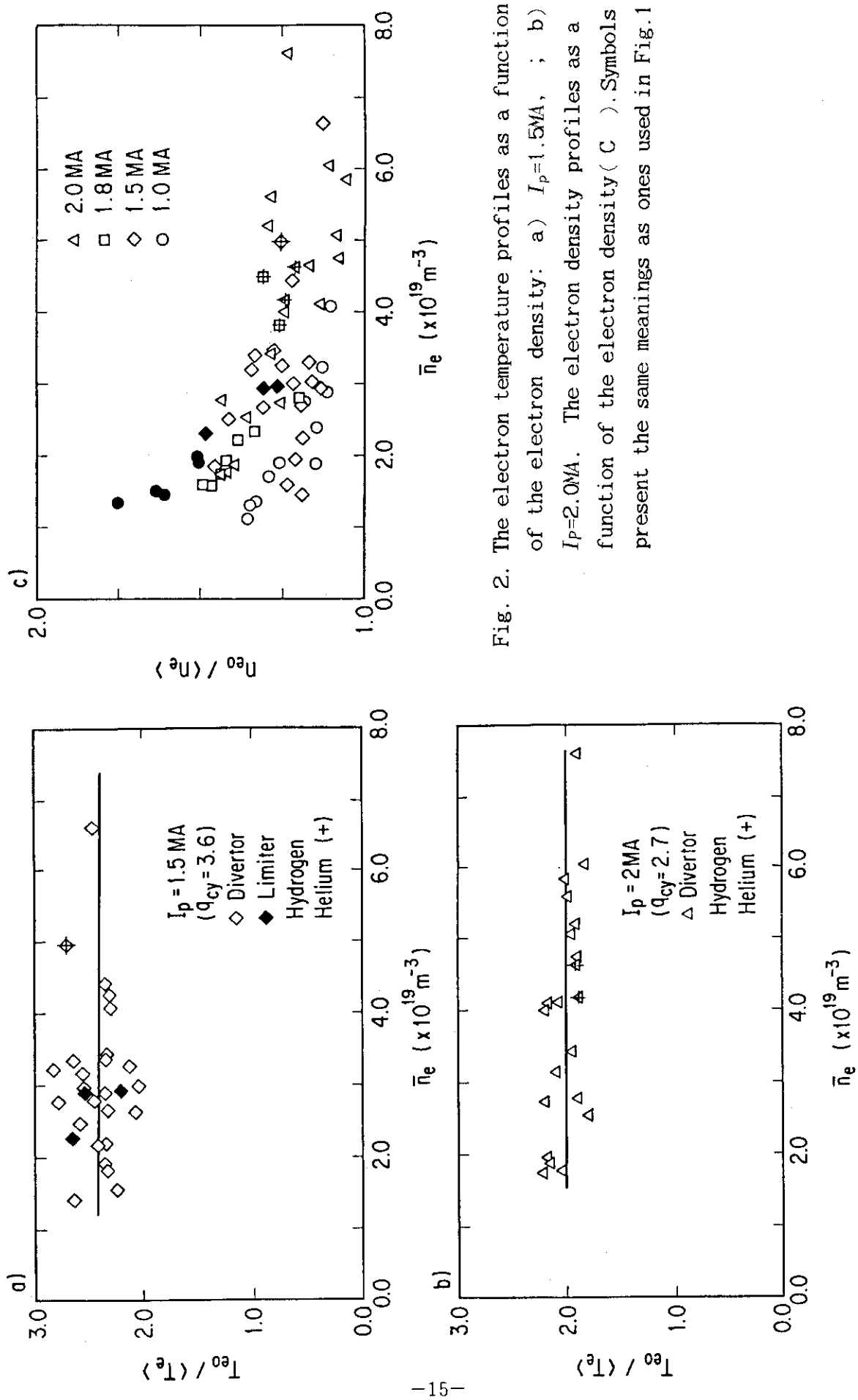

Fig. 2. The electron temperature profiles as a function of the electron density: a) I_p=1.5MA, ; b) I_p=2.0MA. The electron density profiles as a function of the electron density(C). Symbols present the same meanings as ones used in Fig.1.

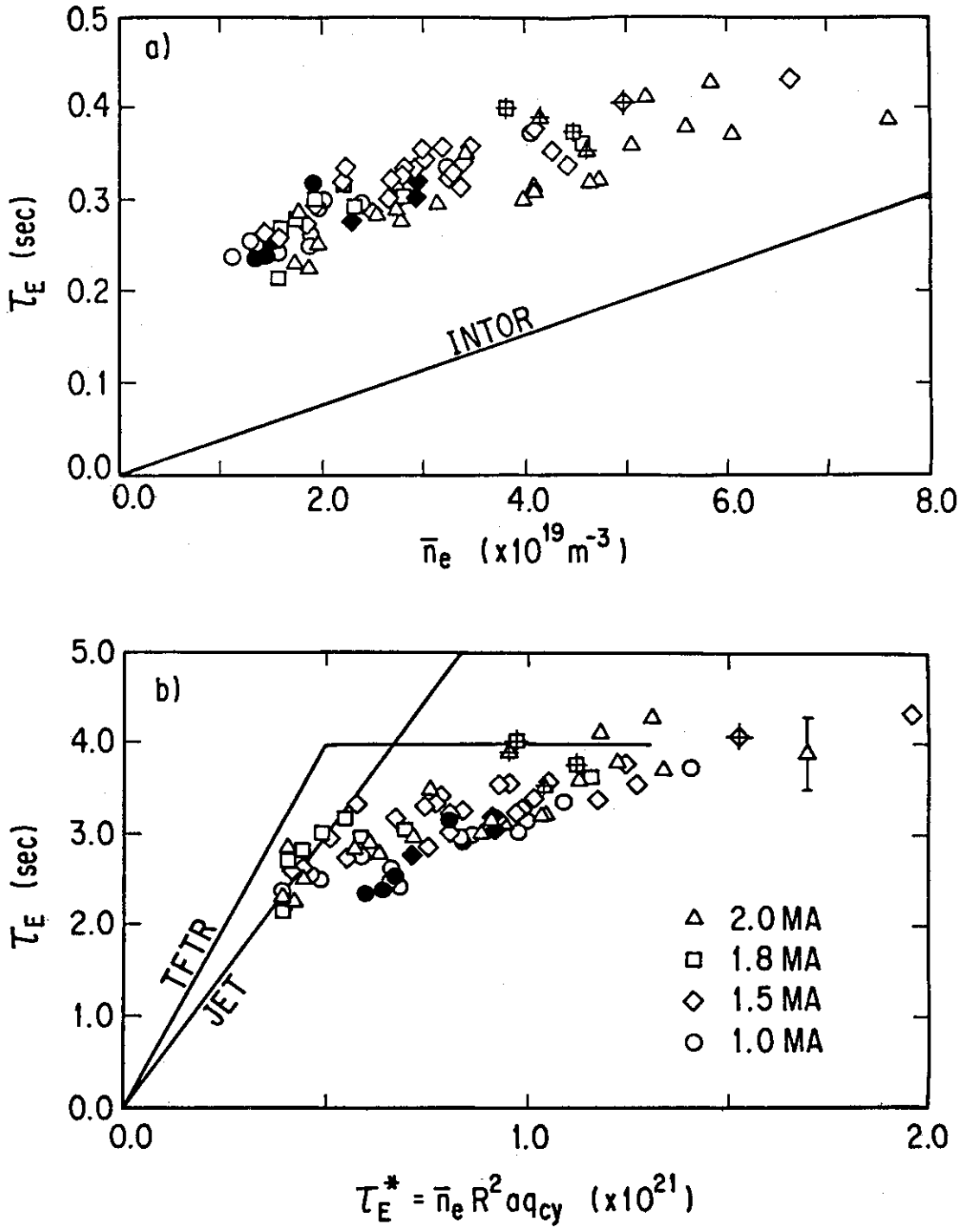

Fig. 3. The energy confinement time versus the line averaged electron density (a) and neo Alcator value scaled with $\bar{n}_e R^2 a q_{cy}$ (b). Symbols present the same meanings as ones used in Fig.1.

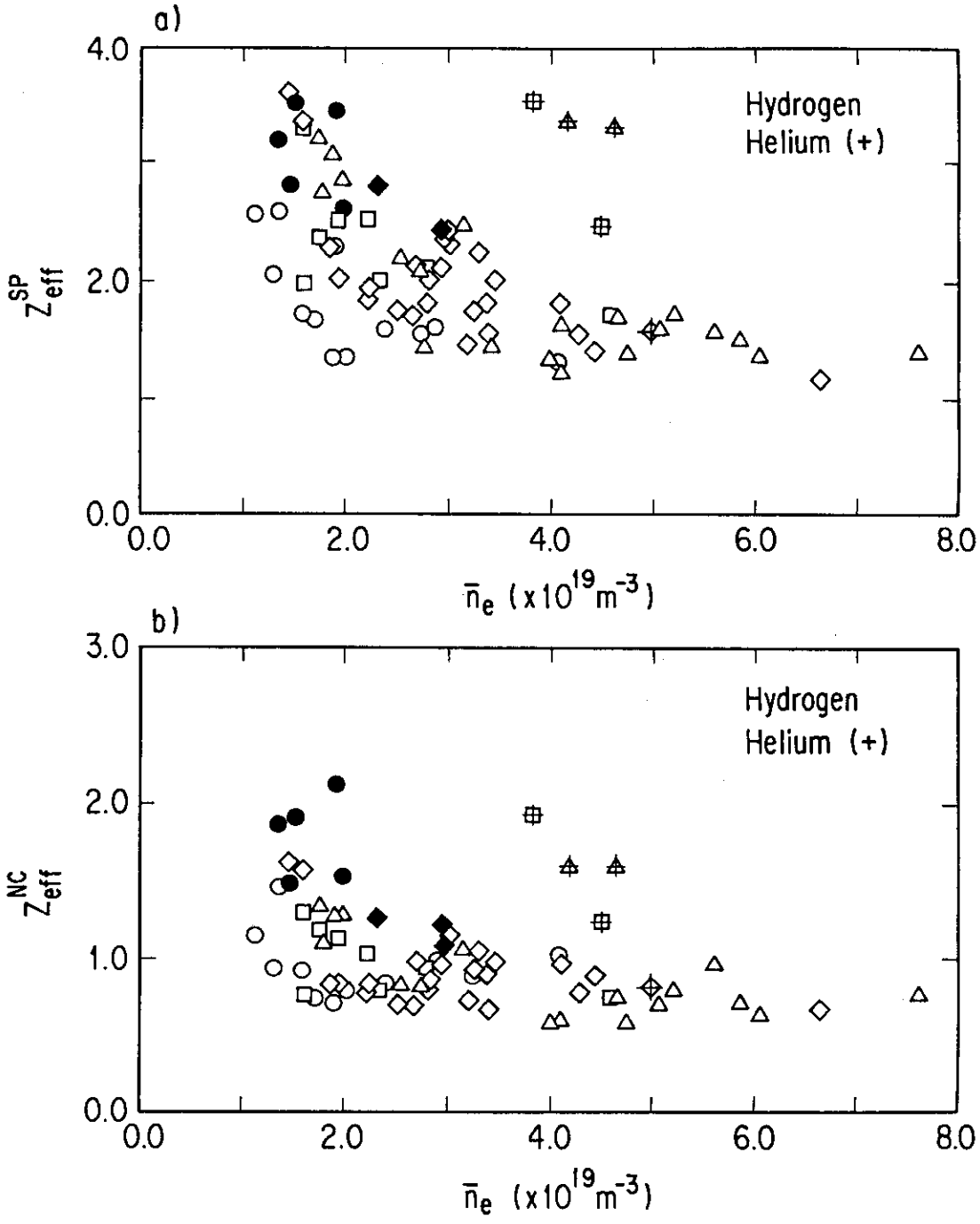

Fig. 4. The resistive Z_{eff} from Spitzer resistivity (a) and from the neoclassical resistivity with trapping correction (b) versus the line averaged electron density. Symbols present the same meanings as ones used in Fig.1.

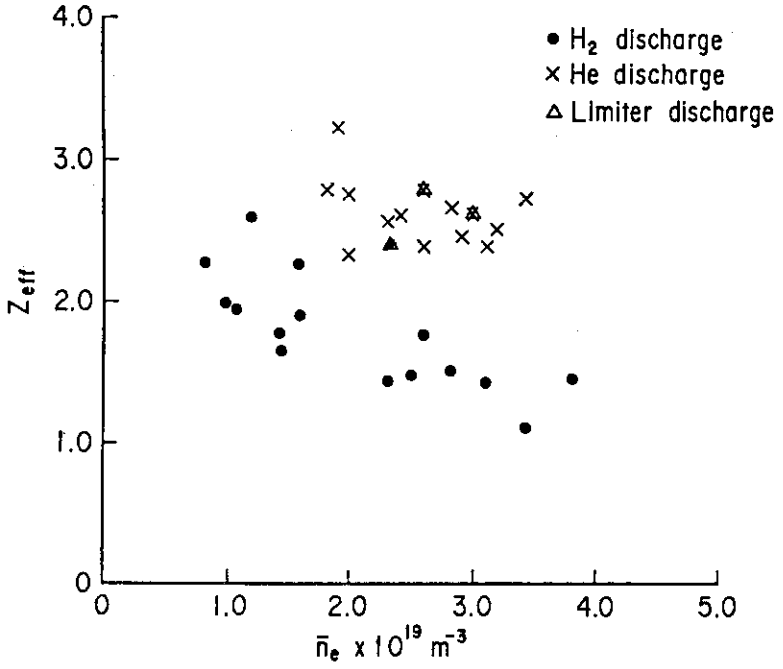

Fig. 5. The value of Z_{eff} measured by visible bremsstrahlung versus the line averaged electron density.

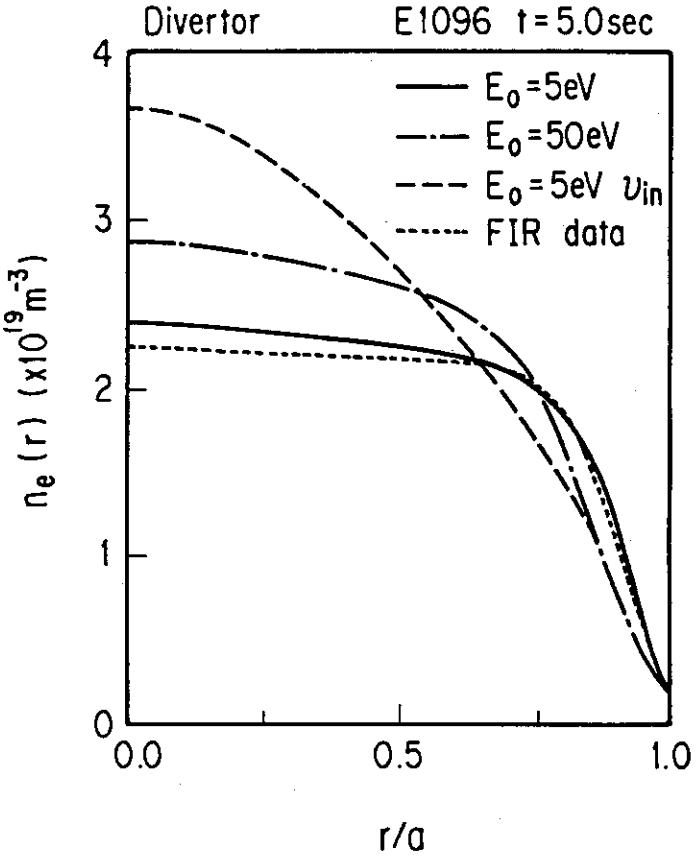

Fig. 6. The electron density profiles computed with empirical transport coefficients and cold neutral energies compared with profile measured by FIR diagnostic (dotted line) for the shot of E1096 divertor discharge. V_{in} is represented by $-2Dr/a^2$.

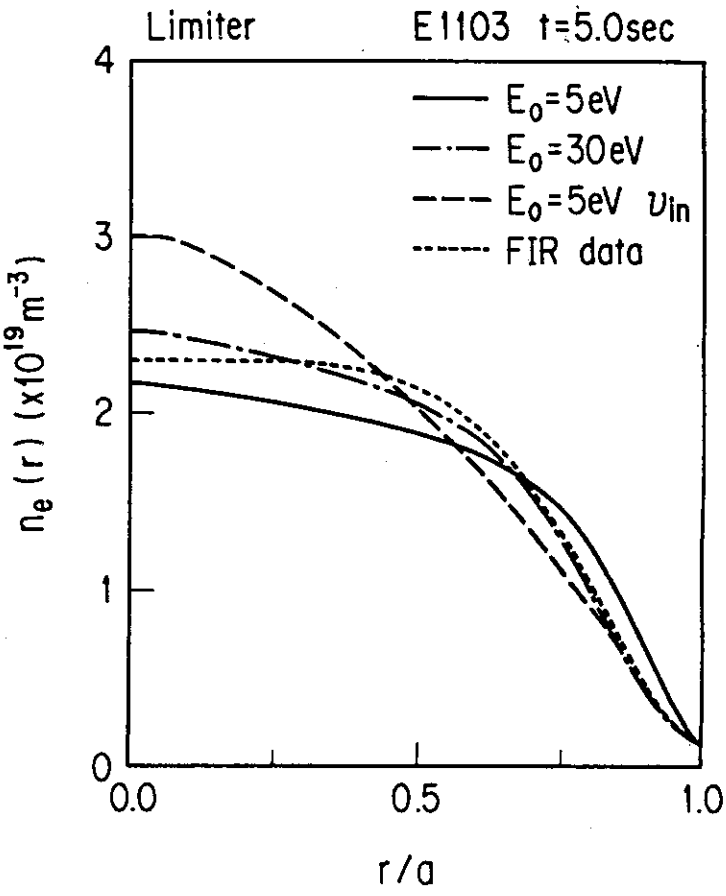

Fig. 7. The electron density profiles computed with empirical transport coefficients and cold neutral energies compared with profile measured by FIR diagnostic (dotted line) for the shot of E1103 limiter discharge. V_{in} is represented by $-2Dr/a^2$.

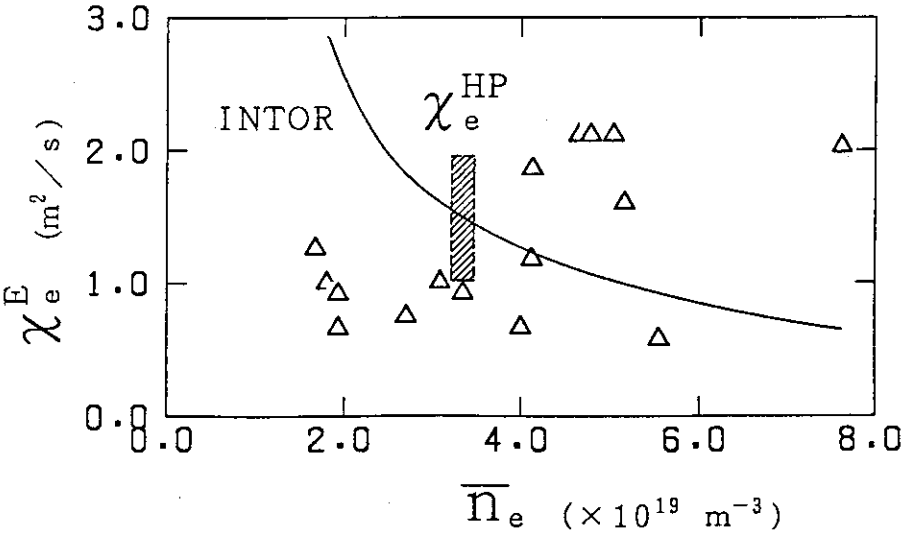

Fig. 8. The electron heat diffusivity χ_e^E estimated at r=a/3 from observed profiles of the electron temperature and density for I_p=1.8MA and I_p=2.0MA. Symbols present the same meanings as ones used in Fig.1. The INTOR scaling of $5\times10^{19}/n_e$ and χ_e^{HP} founded by the heat pulse of the sawtooth are also shown.

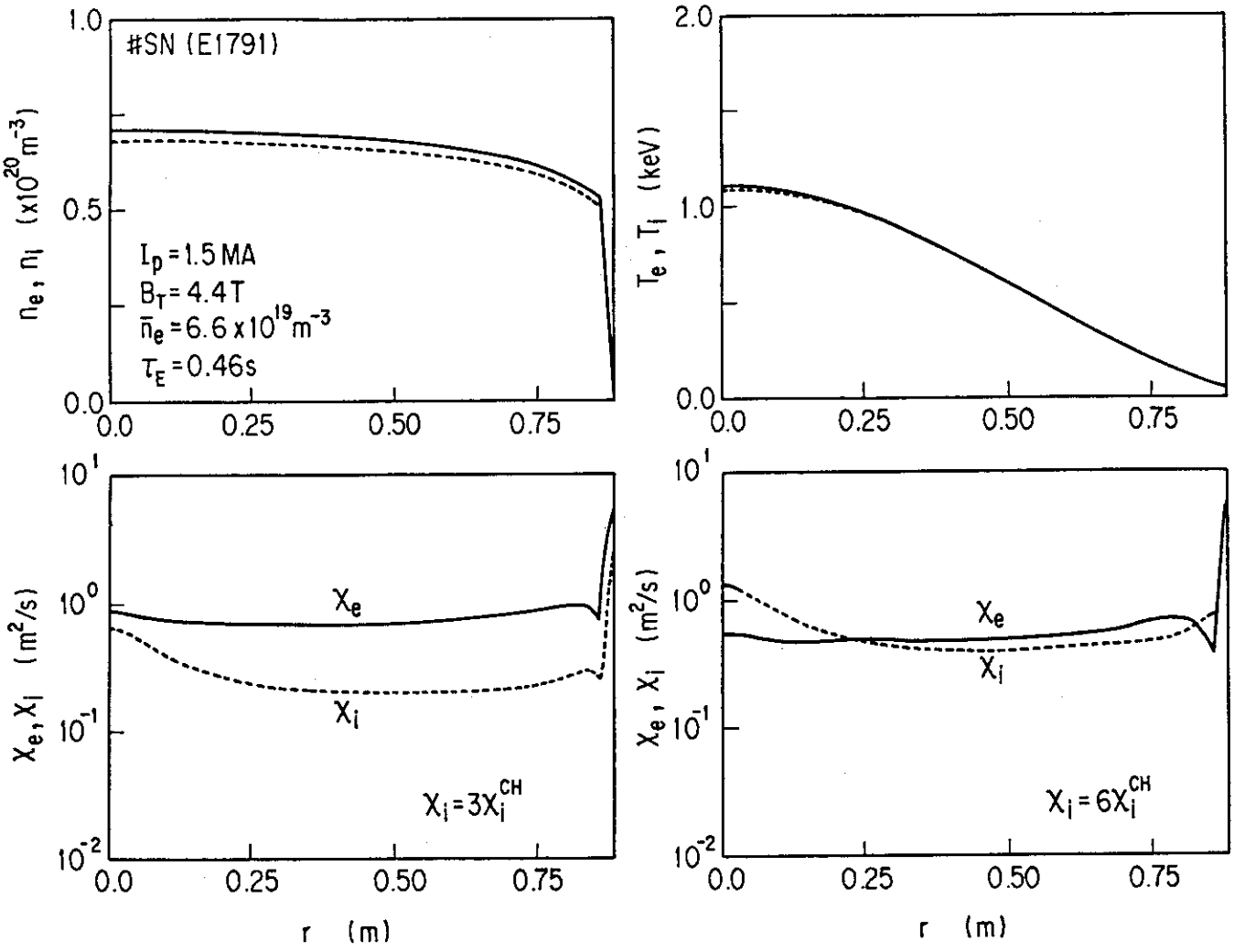

Fig. 9. The comparison of χ_e^E estimated by using the enhancement factor of 3 or 6 for χ_i^{CH}. The experimental profiles of the electron density and temperature for the shot of E1791 with I_p=1.5MA and $\bar{n}_e$=6.6×10$^{19}m^{-3}$. The calculated profiles of the ion density diluted with assumed carbon impurity denoted in a dotted line and the ion temperature from χ_i^{CH} with the multiplication factor denoted in a dotted line.

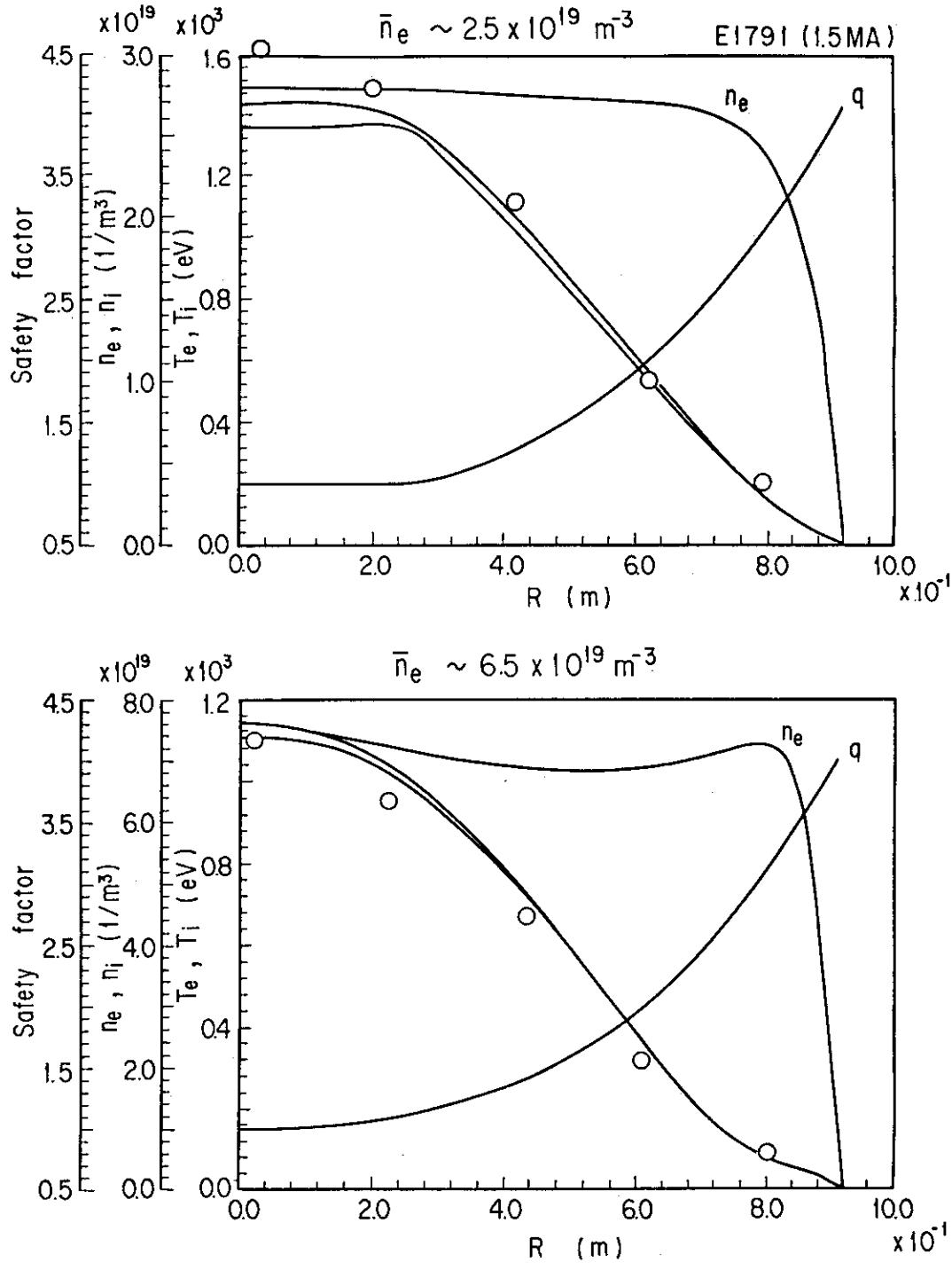

Fig.10. The profiles of electron temperature, ion temperature, electron density and safety factor q calculated with the empirical transport coefficients for the shot E1791 with I_p=1.5MA. Open circles show the electron temperature measure by Thomson scattering.

a) $\bar{n}_e = 2.5 \times 10^{19} m^{-3}$,

b) $\bar{n}_e = 6.5 \times 10^{19} m^{-3}$,

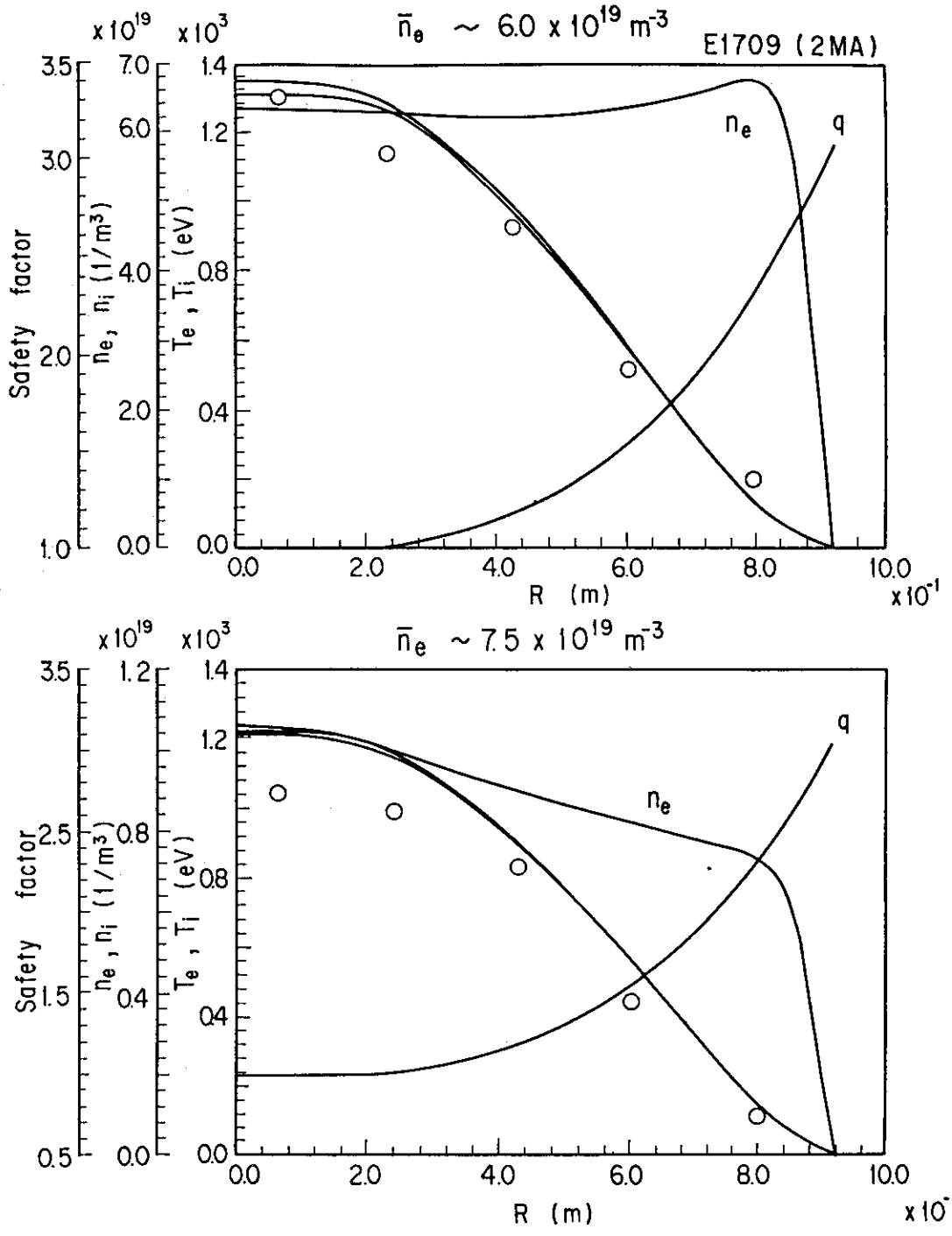

Fig.11. The profiles of electron temperature, ion temperature, electron density and safety factor q calculated with the empirical transport coefficients for the shot E1709 with I_p=2.0MA. Open circles show the electron temperature measured by Thomson scattering.

a) $\bar{n}_e$=6.6×10^{19}m^{-3},

b) $\bar{n}_e$=7.5×10^{19}m^{-3},

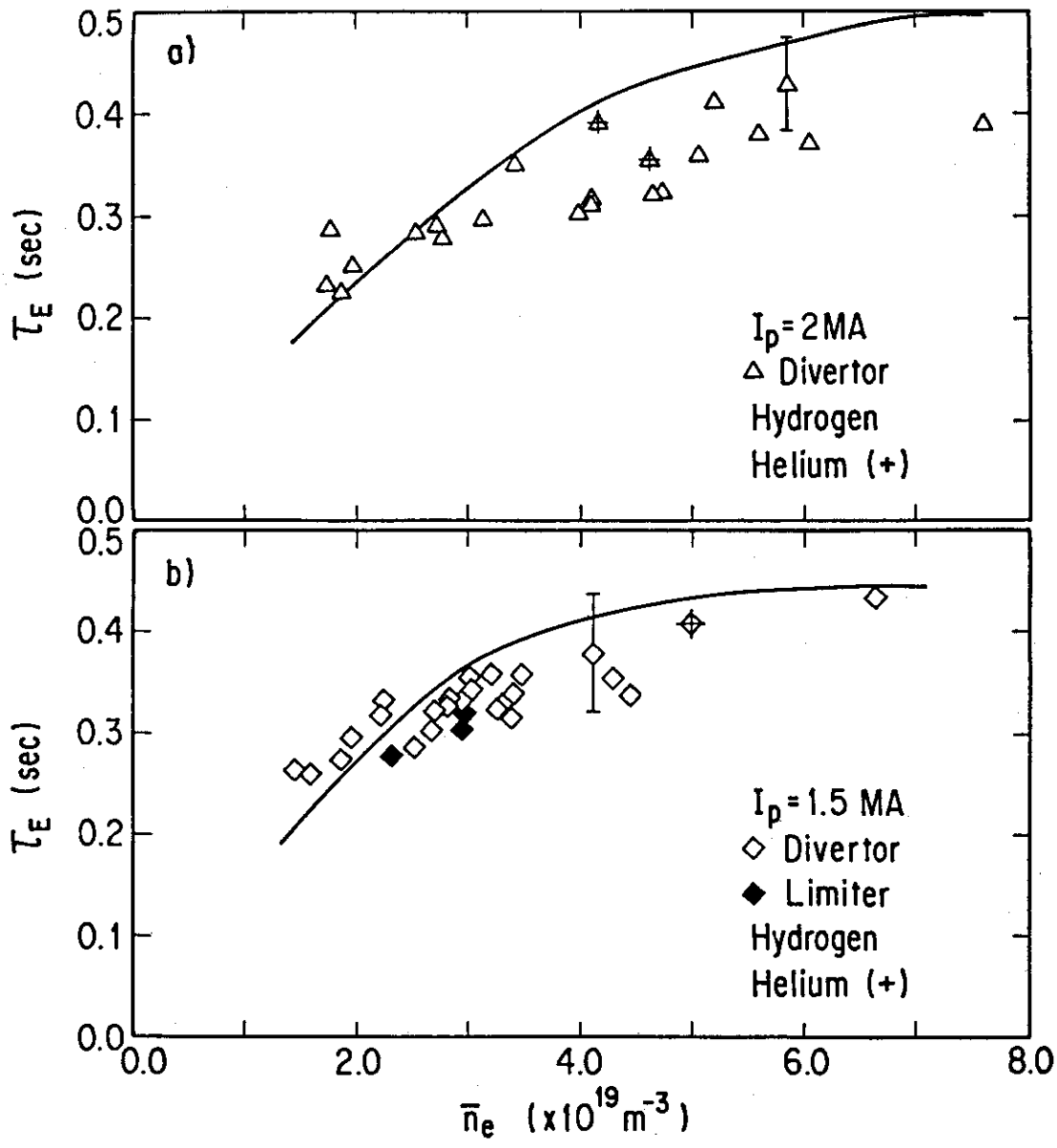

Fig.12. τ_E versus $\bar{n}_e$, comparing with INTOR scaling τ_E (a) and the calculated τ_E (b) ; I_p=1.5MA, (c) ; I_p=2.0MA. Symbols present the same meanings as ones used in Fig.1.

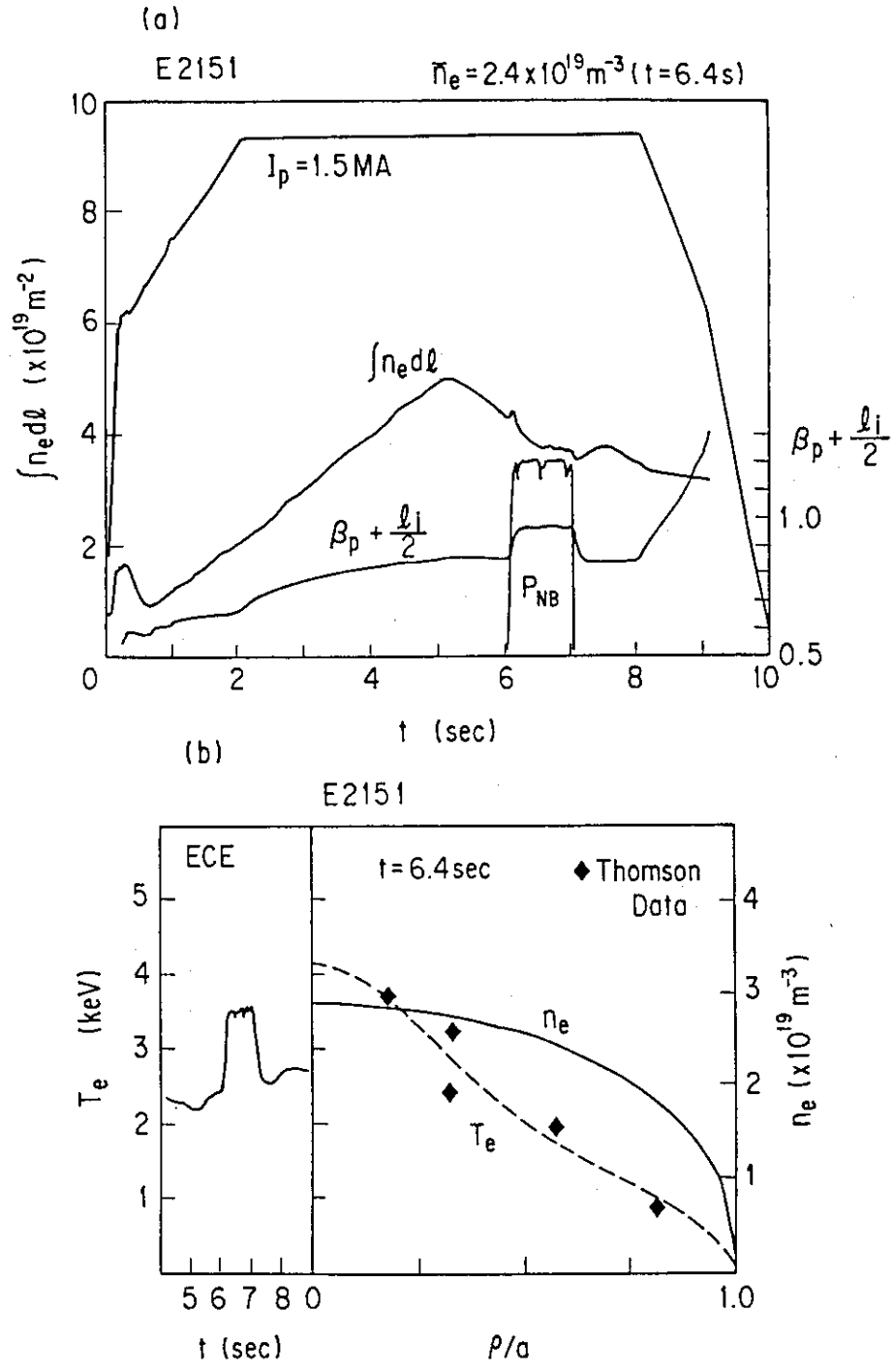

Fig.13. Time evolution and radial profile of the plasma parameters for the relatively high density discharge with 10 MW NBI heating. (a) the plasma current I_P, the line-integrated electron density $\int n_e dl$ and the beta value $\beta_p + 1/2 l_i$ estimated by the magnetic fitting code. (b) The time evolution of the central electron temperature measured by ECE, the density profile obtained from 3-ch FIR data and the electron temperature profile measured by Thomson scattering at t=6.4 sec.

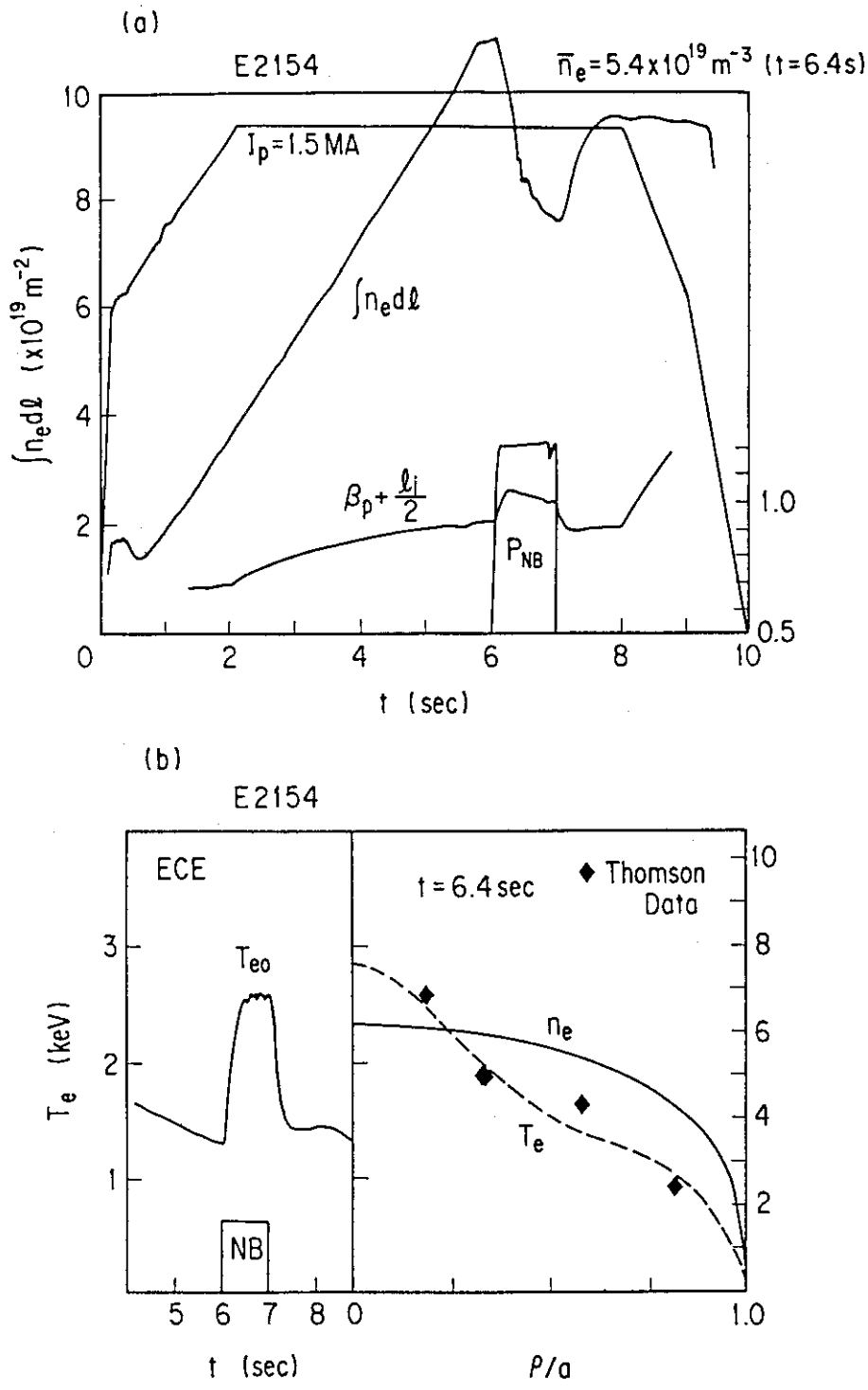

Fig.14. Time evolution and radial profile of the plasma parameters for the low density discharge with 10 MW NBI heating.

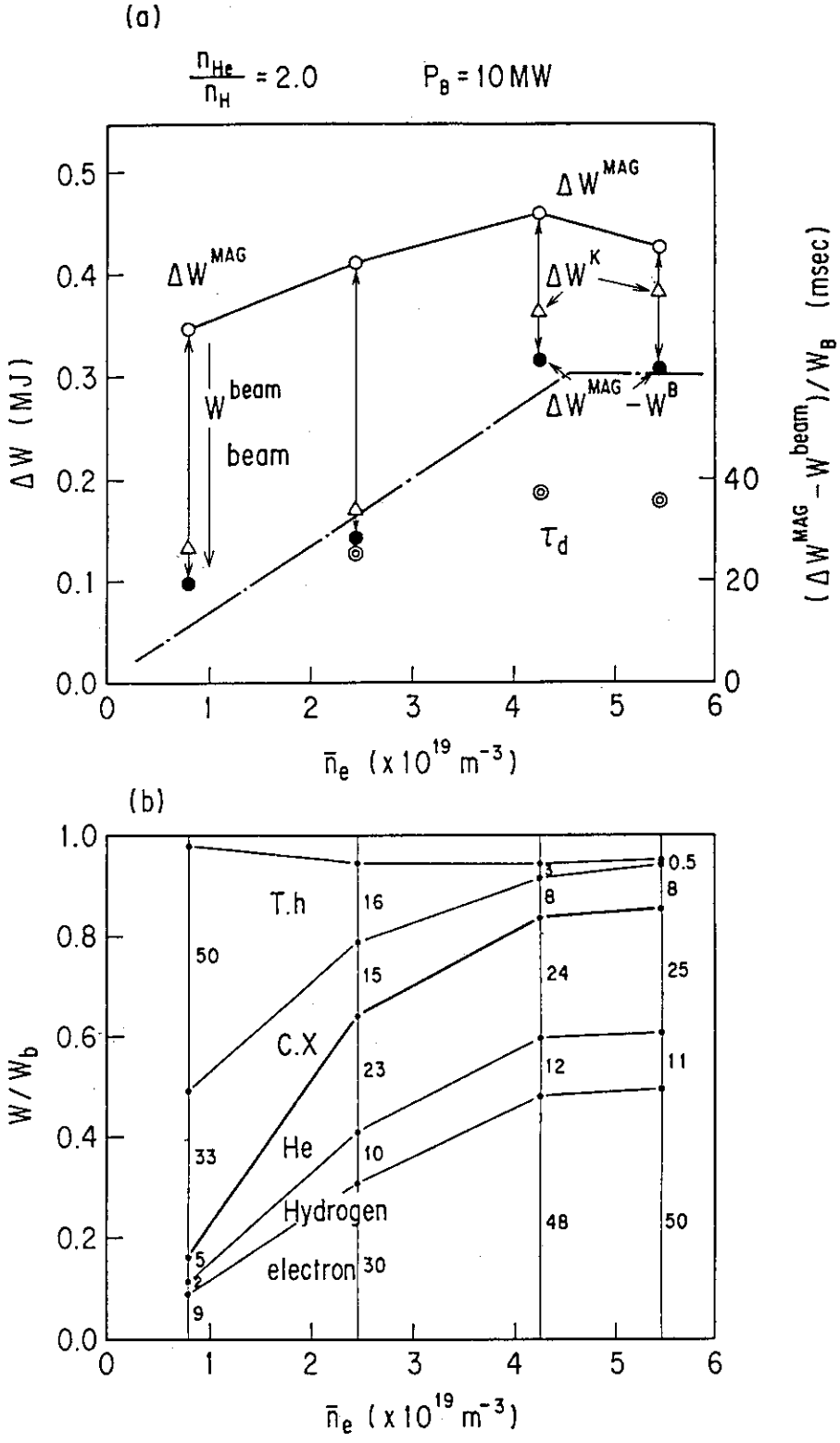

Fig.15. The density dependence of the incremental stored energy and the partition of the beam power for the helium discharge with 10 MW NBI heating.

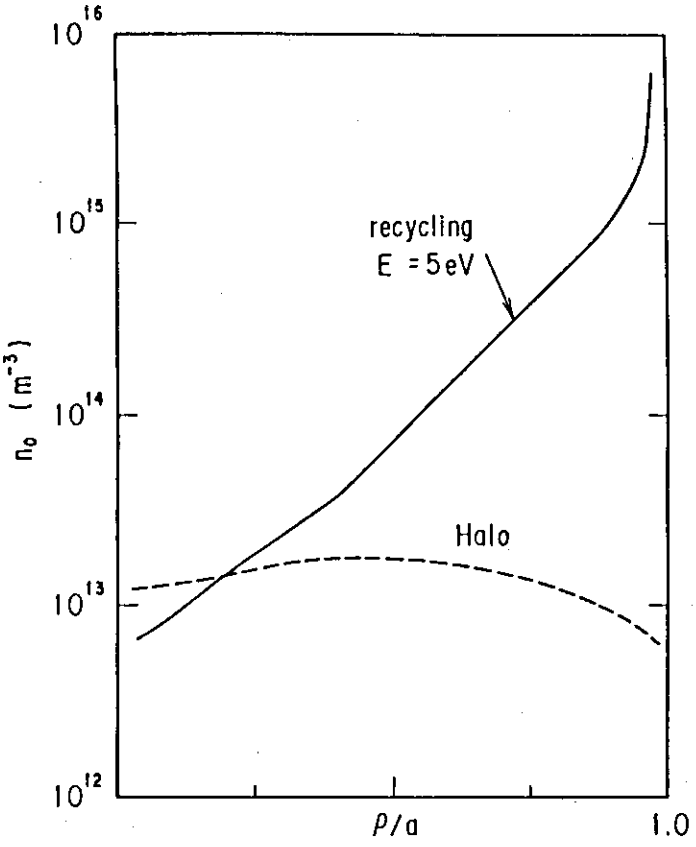

Fig.16. The density profile of recycling neutral and halo neutral

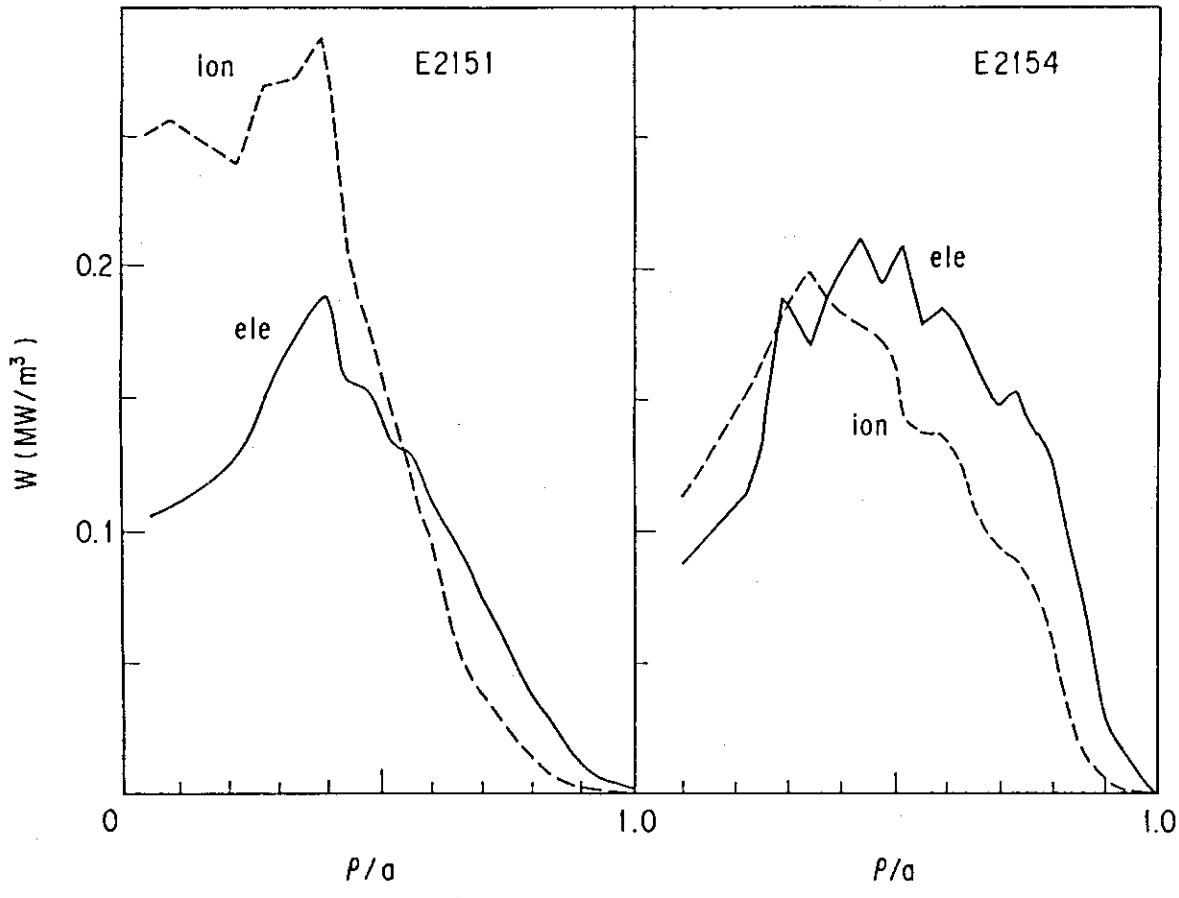

Fig.17. The power deposition profile calculated by OFMC code for E2151 and E2152 discharge.

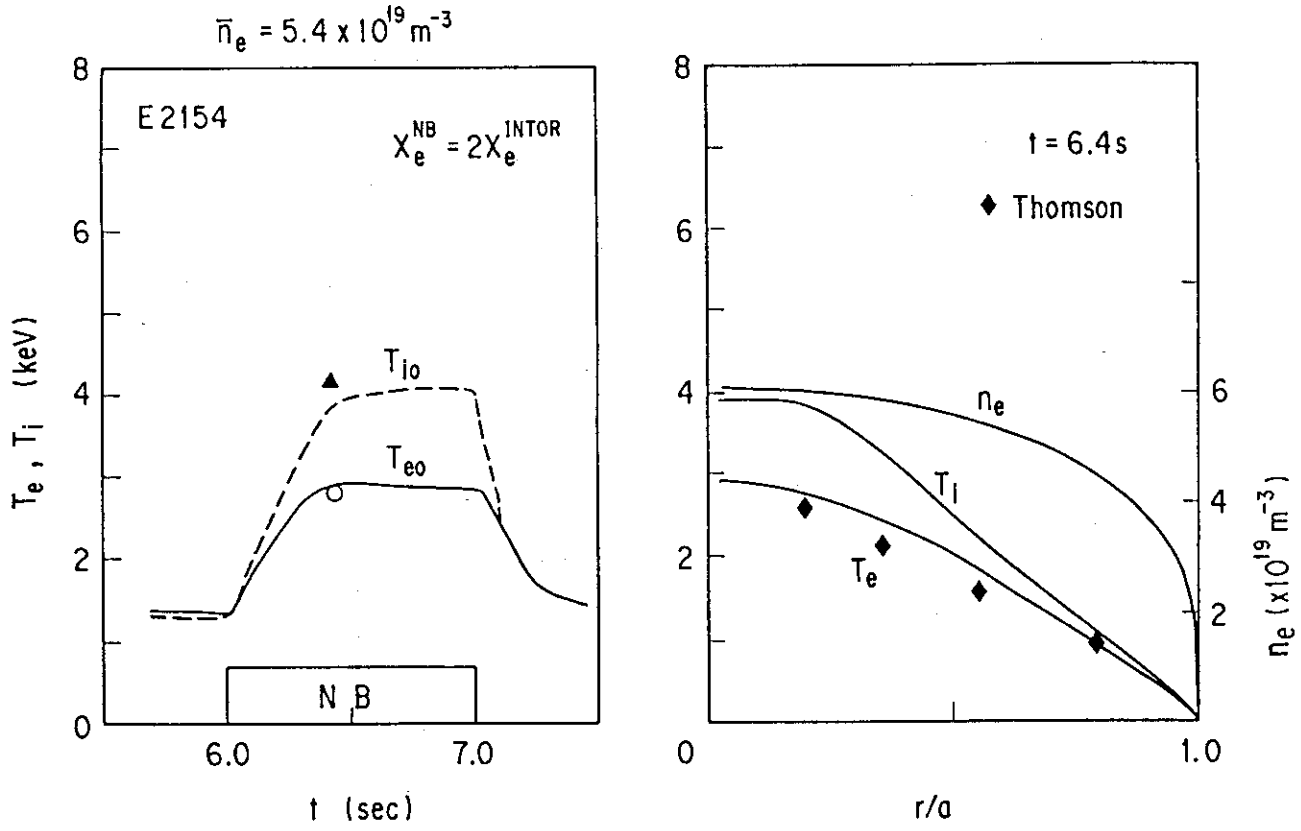

Fig.18. The simulation result for E2154 discharge ($\bar{n}_e = 5.4 \times 10^{19} m^{-3}$) using the enhanced electron heat diffusivity $\chi_e^{NB} = 2 \times \chi_e^{INTOR}$ during NBI heating phase.

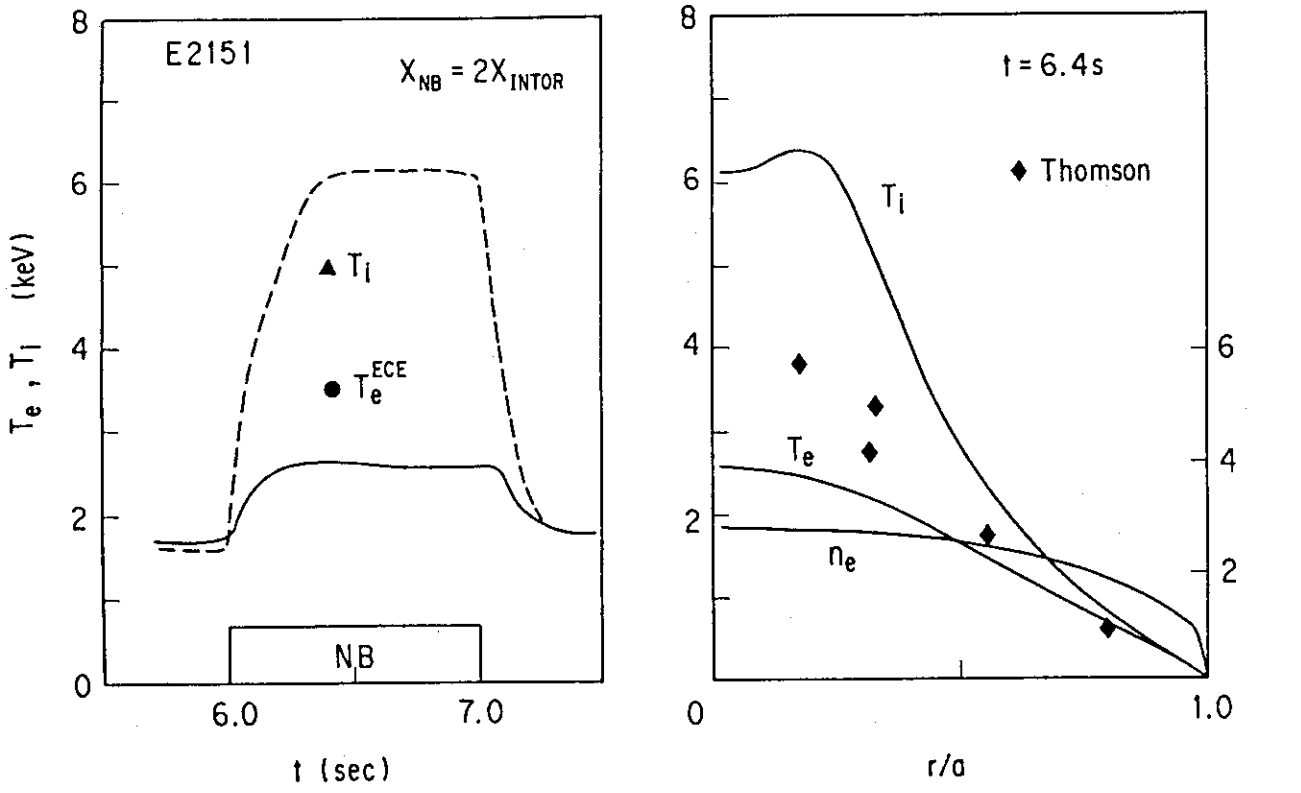

Fig.19. The simulation result for E2151 discharge ($\bar{n}_e = 2.4 \times 10^{19} m^{-3}$) using the same anomalous transport of E2154 simulation.

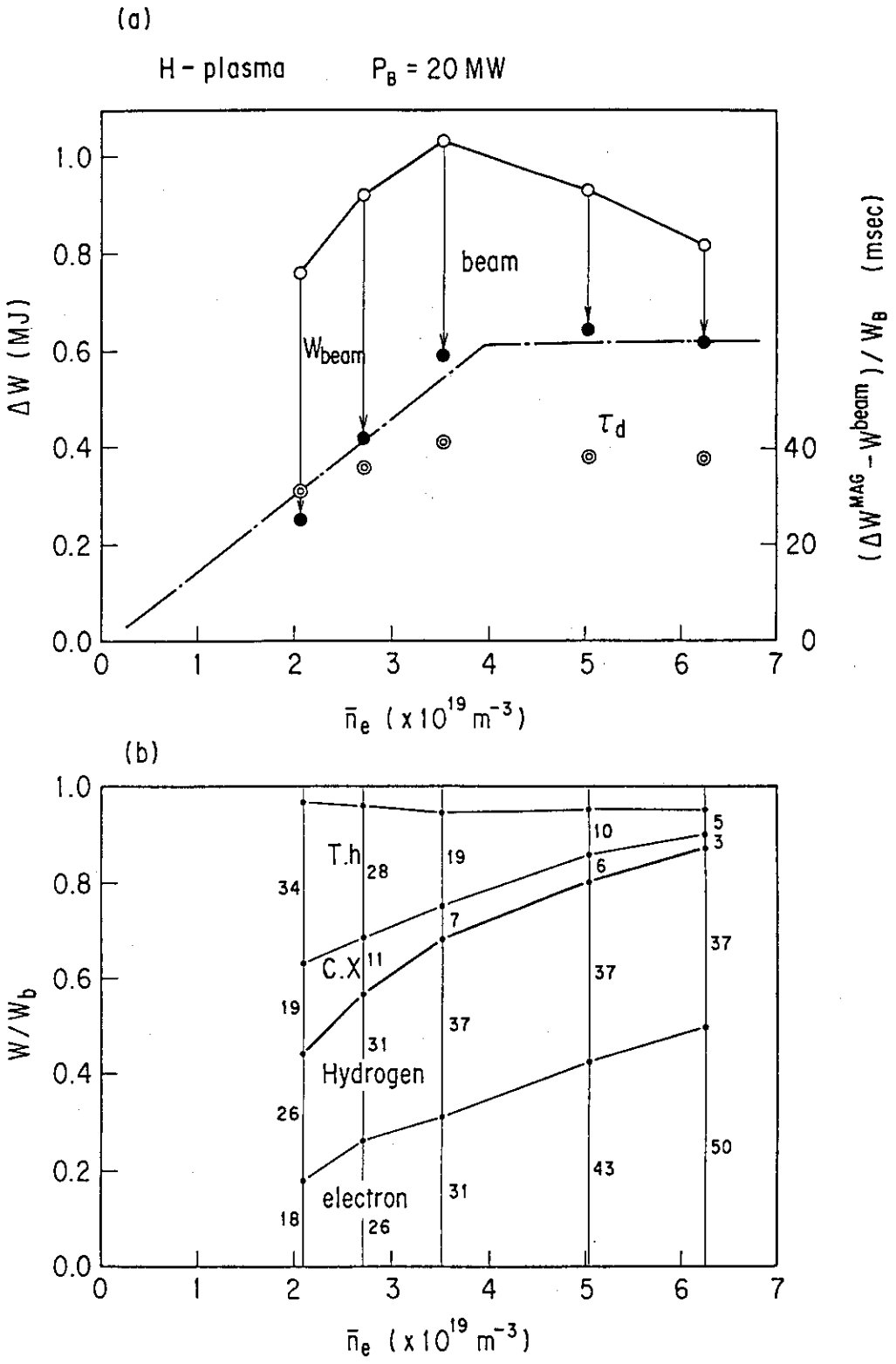

Fig.20. The density dependence of the incremental stored energy and the partition of the beam power for the hydrogen discharges with 20 MW NBI heating.

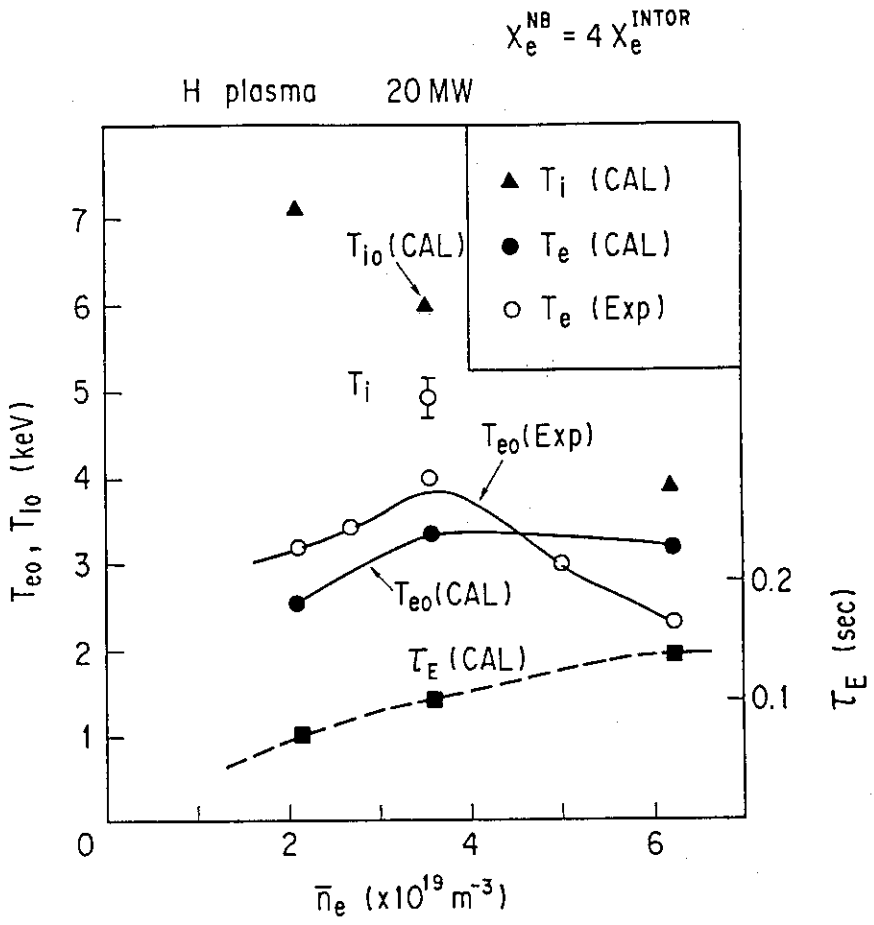

Fig.21. The simulation results for a series of the hydrogen discharge with 20 MW NBI heating and the experimental data. The electron heat diffusivity χ_e^{NB} is enhanced by a factor 4.